Sample analysis to determine accident progression

■ 1. Introduction

Analysis of samples collected inside and outside 1F Units 1-3 PCVs revealed particles containing U. The U-containing particles are thought to have originated from the accident progression in Units 1-3, and since the compositions and structures of the particles might retain information about the vicinity of the particles at the time they were formed, detailed analysis of the site samples could be used to understand the progression of the accident. In addition, silica particles containing Cs (insoluble cesium particles) have been found in the environment, and these solid particles might also contain information on accident progression.

Figure 1 shows how radioactive particles and fuel debris were formed and migrated as the accident progressed. From a normal pre-accident state, the fuel overheated due to the depletion of cooling water, causing the fuel and structural materials to react and melt. In the course of the accident progression, the molten and fallen fuel then cooled and solidified and was distributed as fuel debris in the lower part of the pressure vessel and the bottom of the containment vessel. Most of the U in the fuel is considered to have formed fuel debris, but some of it formed particles from molten droplets in the pressure vessel and containment vessel, or formed particles by evaporation and condensation of U. These particles migrated and are now widely acting as sources of α-contamination in the buildings. In the figure the formation and spreading mechanism is indicated for U-containing particles that have undergone the melting and solidification process by red circles, and for U-containing particles that have undergone the evaporation and condensation process by orange circles. Particulate fission products (FPs) are indicated by green circles. These radioactive particles are considered to have different compositions and microstructures depending on the atmosphere in the reactor at the time of their formation and the cooling conditions leading up to particle formation. Therefore, the characteristics of their composition and microstructure are considered to contain information on the accident progression and the properties of the fuel debris.

Detailed analysis of samples from the 1F site regarding solid particulates is being conducted in collaboration with the subsidized projects "Advancement of comprehensive in-vessel status understanding" and "Development of analysis and estimation techniques to understand the properties of fuel debris." The analysis results have been published in the Decommissioning, Contaminated Water and Treated Water Team Meeting Secretariat Meetings [1-4], in the Decommissioning Research Infrastructure Database (debrisWiki) [5], which is being developed in cooperation with JAEA, and in the JAEA report [6]. This attachment describes the contents that are considered important from the viewpoints of the study on debris location, which is important input for decommissioning work and understanding of the accident progression, in relation to the issue "Common-10: Core Damage Status and Debris Location" in Appendix 2.

The efforts on the sample analysis are listed as a common attachment for Units 1-3, because

the analysis is considered effective not only for specific interpretation about Units 1-3 but also for interpretation throughout Units 1-3, and because it includes many contents in the field of materials and chemistry that do not fit in the attachments for each unit separately.

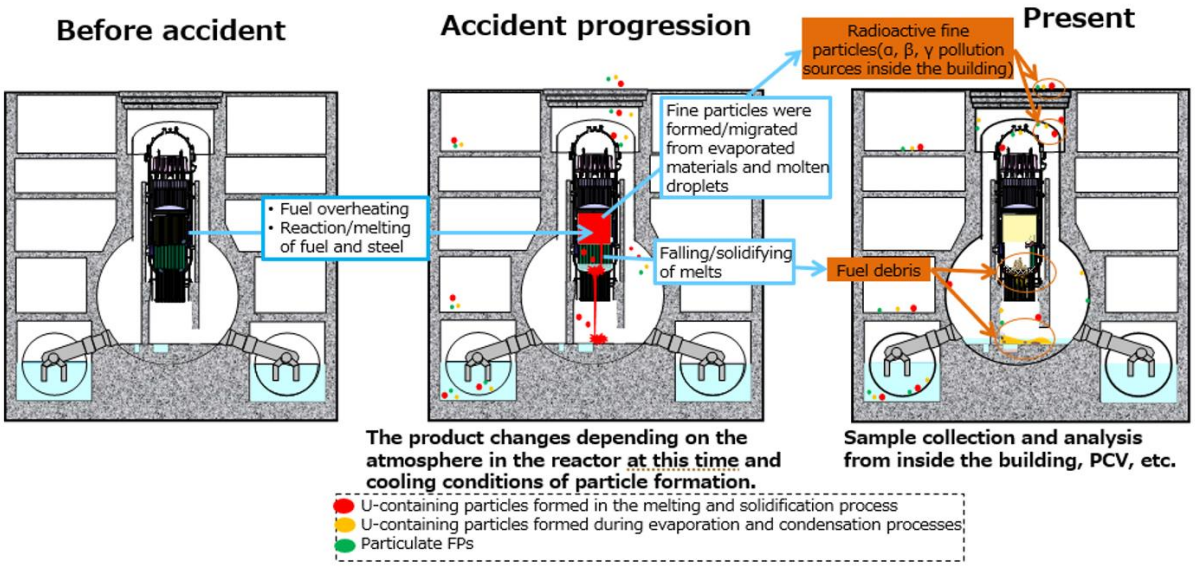

Figure 1 Relationship between properties of radioactive particles and fuel debris, and accident progression

■ 2. Sample analysis

■ 2.1. Target of analysis

In this study, the main target of analysis was samples obtained through the decommissioning process of 1F that had a clear origin and relatively high radiation dose, in order to estimate the properties of the fuel debris and to understand the progress of the accident. Table 1 lists the acquired samples and Figure 2 shows their approximate acquisition locations.

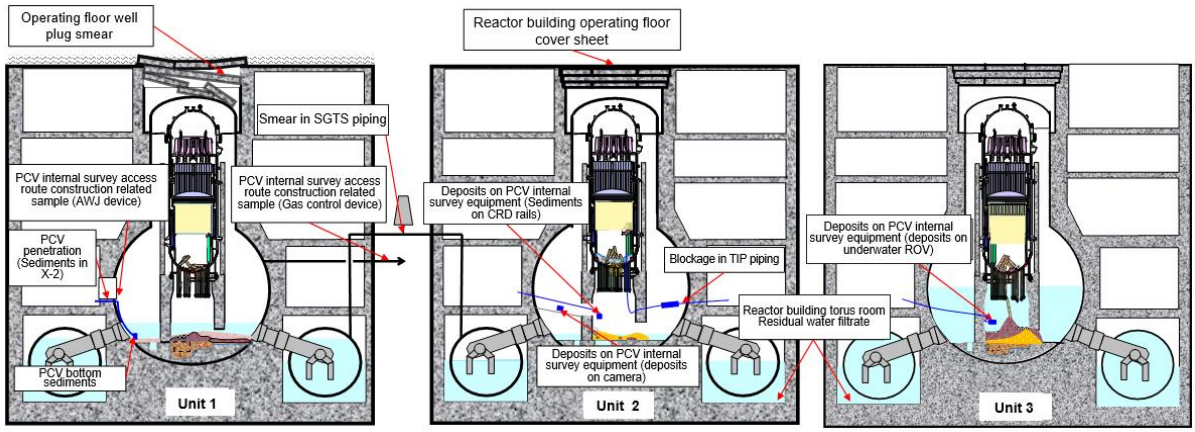

Figure 2 Overview of sample acquisition locations

Table 1 Acquisition samples

Unit	Sample name	Sampling time
1	PCV bottom sediments	Apr 2017
1	PCV penetration (Sediments in X-2)	Jun 2019
1	Operating floor well plug smear	Aug-Jul 2019
1/2	Smear in SGTS piping	May 2020
1	PCV internal survey access route construction related sample (AWJ device)	Mar 2020
1	PCV internal survey access route construction related sample (Gas control device)	Jun 2019
2	Deposits on PCV internal survey equipment (Sediments on CRD rails)	Feb 2017
2	Reactor building operating floor cover sheet	Mar 2014
2	Blockage in TIP piping	Jul 2013
2	Deposits on PCV internal survey equipment (deposits on camera)	Jan 2018
2	Reactor building torus room residual water filtrate	May 2019
3	Deposits on PCV internal survey equipment (deposits on underwater ROV)	Jul 2017
3	Reactor building torus room residual water filtrate	May 2019

In the next section, based on the analysis results of some of the samples shown in Table 1, the details of the study are discussed from the viewpoint of understanding the debris distribution and accident progression. Below, A) to D) describe the acquisition status of the samples taken up. In addition, the results of A) sample were used in section 3.1, B) sample in 3.4, C) sample in 3.5, and D) sample in 3.6 to 3.8.

A) Units 2 and 3 reactor building torus room stagnant water filtrate [3].

Since relatively high concentrations of α-nuclides have been confirmed in the stagnant water in the reactor buildings of Units 2 and 3, filtration tests were conducted to ascertain the degree to which α-nuclides, most of which are estimated to exist in particle form, can be removed by the filter in order to determine their properties before proceeding with water treatment. The stagnant water collected from the reactor building torus rooms of Units 2 and 3 in May 2019 was filtered through a 0.1 μm filter. A schematic diagram of the locations where the stagnant water was collected is shown in Figure 3, and a photograph of the collected stagnant water is shown in Figure 4. Since the stagnant water in Unit 2 was collected in the deeper part of the trench, turbidity, assumed to be sludge, was observed at the bottom of the water. Table 2 shows the total α concentration in the water before and after filtration, and the removal rate calculated from the concentration. The total α concentration in the stagnant water was measured and found to be relatively high, indicating that more than 90% could be removed, although some remained in the stagnant water. The filter was used as a sample to analyze the particles and other substances removed in this filtration test.

Table 2　Residual water filtration test results in the reactor building torus rooms of Units 2 and 3

Sampling location	Original water (before filtration) Total α concentration [Bq/L]	Concentration after filtration (0.1μm) [Bq/L]	Removal efficiency
Unit 2 Reactor building	2.61×10^5	9.54×10^2	99.6%
Unit 3 Reactor building	1.50×10^3	1.12×10^2	92.5%

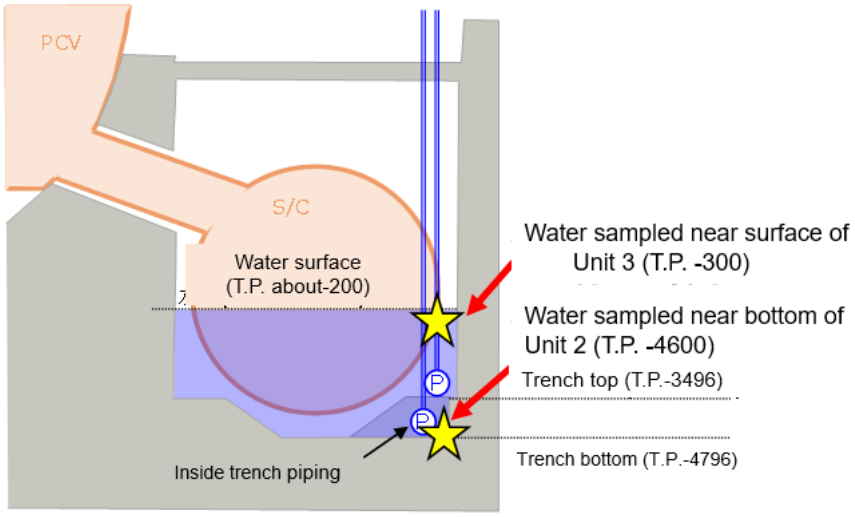

Figure 3　Units 2 and 3 reactor building torus room stagnant water sampling locations

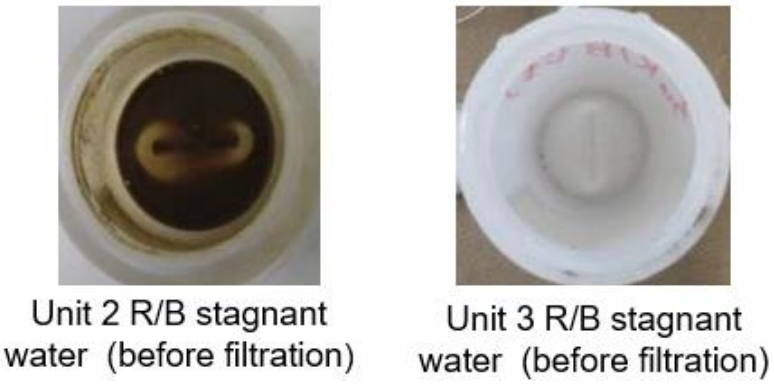

Figure 4. Stagnant water samples

B)　Sediments at the bottom of the Unit 1 PCV [1,2].

When the permanent monitoring instrument was reinstalled after the PCV internal investigation conducted in April 2015, sediments in the PCV stagnant water were observed to be whirled up. In order to identify the sediments and examine retrieval and disposal methods, in April 2017 PCV stagnant water was collected by dropping a water suction hose from the

PCV penetration (X-100B) to the bottom of the PCV and suctioning it up with a pump (Figure 5). Based on the video of the sampling, it is believed that, in addition to the PCV stagnant water, suspended material on top of the hard layer deposited at the bottom of the PCV was sampled, too.

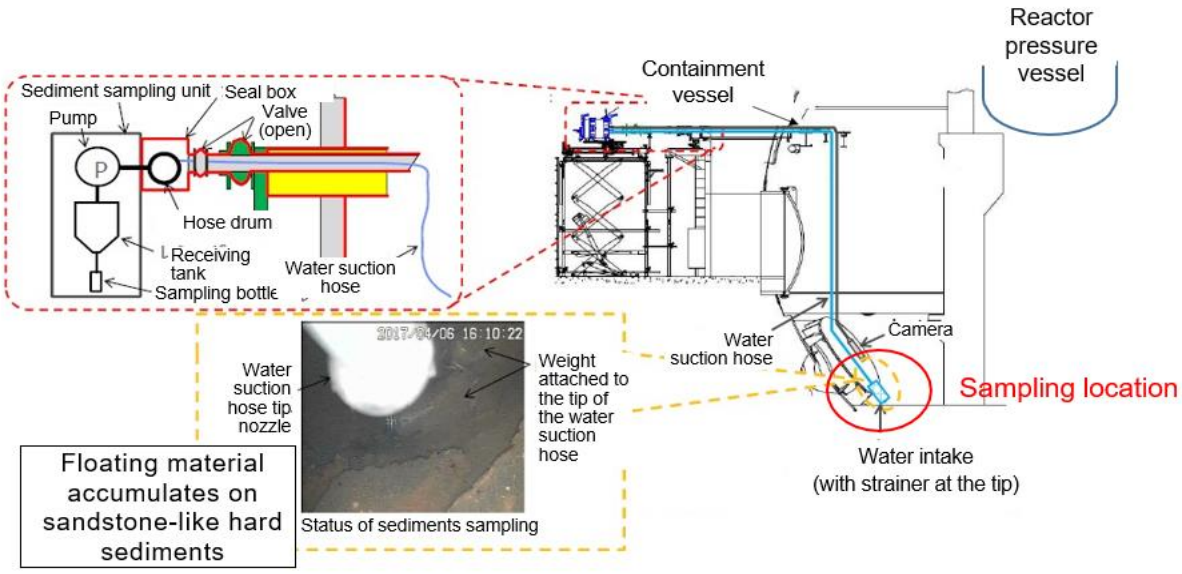

Figure 5 Overview of sampling equipment (bottom sediment of Unit 1 PCV)

C) Sediments inside the Unit 1 PCV penetration (X-2) [3].

In April to May 2019, the outer door was drilled as part of the work to construct an access route to investigate the inside of the PCV from the Unit 1 PCV penetration (X-2). The PCV penetration (X-2) is an airlock for the station staff and has an outer door on the building side and an inner door on the PCV side. When the outer door was drilled and the interior was checked, deposits were found on the floor near the inner door (Figure 6). In order not to interfere with the drilling of the inner door at a later stage, in June 2019 part of the deposits was removed using a jig. The surface of the jig used in this process was wiped with a smear that was used as a sample.

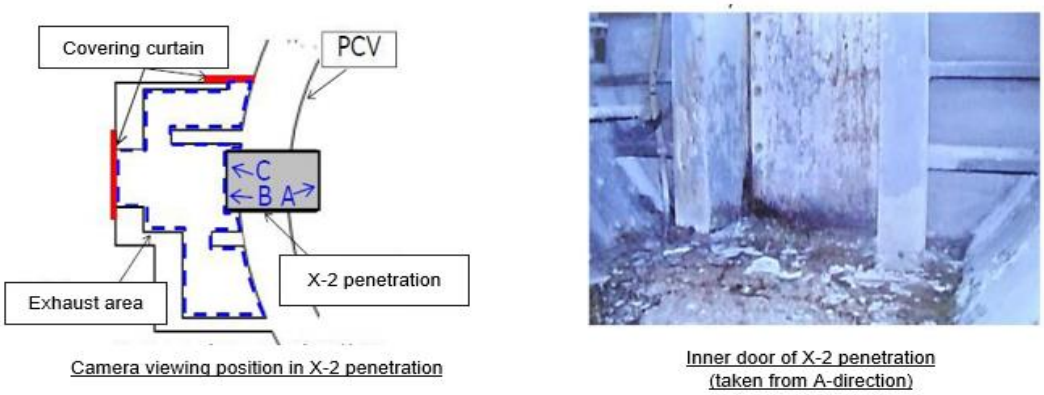

Figure 6 Conditions before removal of sediments in the penetration

D) Unit 2 reactor building operating floor cover sheet [1-3].

The flame-retardant sheet that had been laid on the top floor of the Unit 2 reactor building (operating floor) for the purpose of floor covering before the accident, was sampled by a robot in March 2014. Since no hydrogen explosion occurred in Unit 2 and the ceiling and walls of the reactor building were not significantly damaged, the effects of rainfall and contamination from other units were considered to be small. The sample was considered to have been in the path of radioactive material that was released into the building via the top cover of the PCV and the concrete well plug (shield plug) for shielding directly above it, and therefore it is considered to still have traces of that radioactive material.

■ 2.2. How to proceed with the analysis

Figure 7 shows an example of the analysis flow for the samples used in this study. At JAEA Oarai, mass spectrometry using ICP-MS, α/γ spectral analysis, and electron microscopy using SEM-WDS were performed. SEM/TEM-EDS was used for more detailed analysis at NFD.

Figure 8 shows a more specific method of searching for and observing radioactive particles than in Figure 7. First, a relatively wide elemental distribution (mapping) is obtained by SEM-EDS, and then the high concentration points are searched for, focusing on U (nuclear fuel material) and Cs (fission product). The high concentration points found are observed in more detail by increasing magnification of SEM-EDS, and the areas that are considered suitable as samples for TEM analysis are selected from the viewpoint of analytical needs and sampling feasibility. In TEM observation, in addition to TEM images, elemental analysis using TEM-EDS and electron beam diffraction are used to evaluate microstructure, composition, and crystal structure in detail.

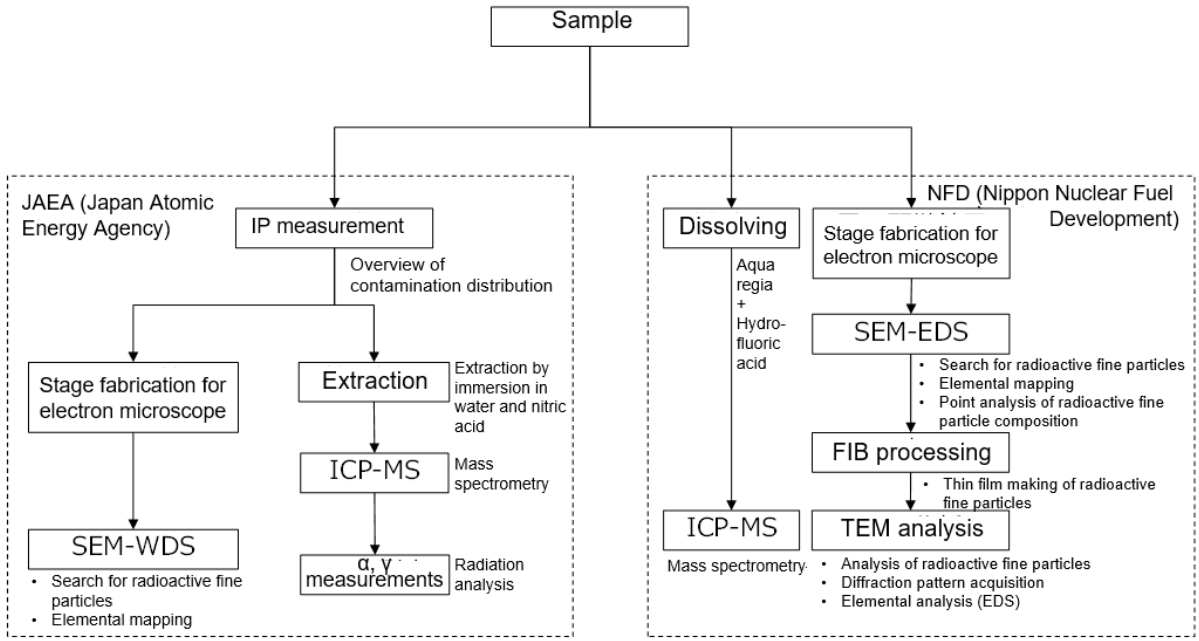

IP, imaging plate; ICP-MS, inductively coupled plasma mass spectrometry;
SEM, scanning electron microscope; EDS, energy dispersive X-ray spectroscopy;
WDS, wavelength dispersive X-ray spectroscopy; FIB, focused ion beam;
TEM, transmission electron microscope

Figure 7 Example of sample analysis flow

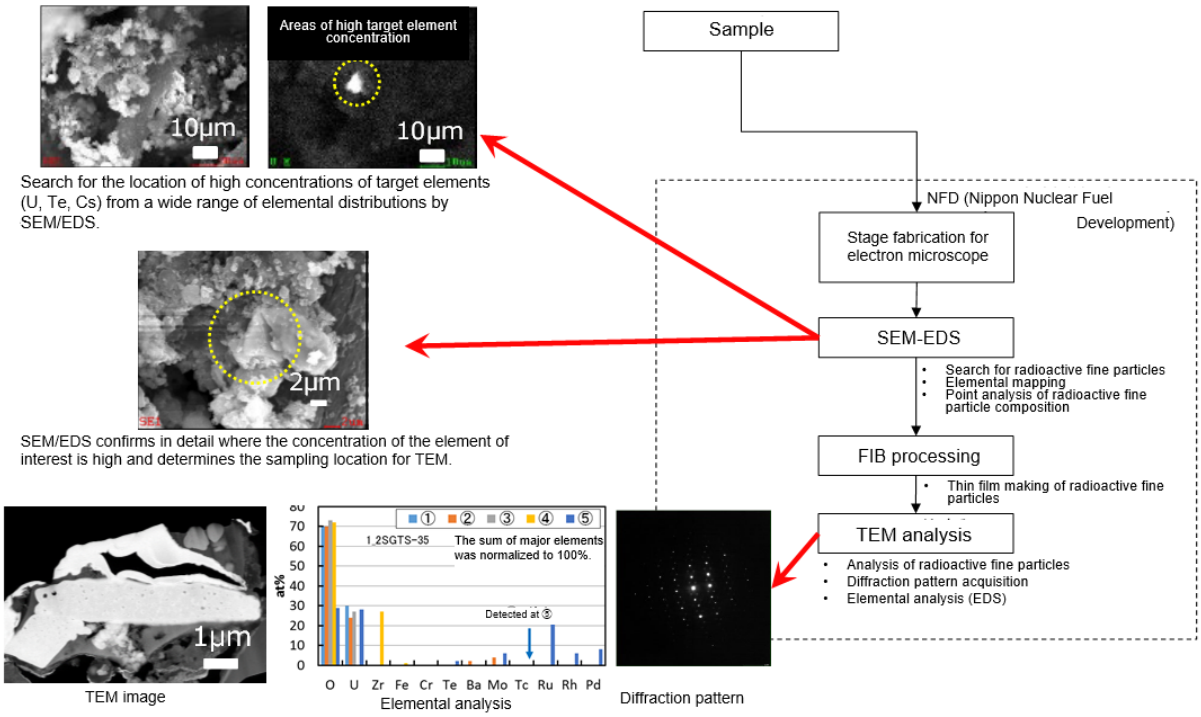

From the focus position, a TEM sample is processed using FIB, and the microstructure, composition, and crystal structure of the sample are measured by TEM/EDS/electron beam diffraction.

Figure 8 Example of analysis flow (SEM/TEM-EDS analysis)

■ 3. Estimation of formation process of radioactive fine particles

In each part of this section, after presenting the results of sample analysis obtained at the analytical facility, the results of studies that are considered important from the viewpoint of understanding the progression of the accident and debris distribution are described.

■ 3.1. U-containing particles in stagnant water in buildings

As mentioned above, filtration of water samples near the bottom of the Unit 2 reactor building torus room and near the water surface of the Unit 3 reactor building torus room using 0.1 μm filter paper resulted in removal of 99.6% of total α in Unit 2 and 92.5% in Unit 3. This suggests that most of the α contamination sources exist in particle form. In order to confirm the presence of these particles, the filter paper used for filtration was observed by SEM-WDS. SEM-WDS mappings of U, Pu, and Zr in Units 2 and 3 are shown in Figures 9 and 10.

In Unit 2, U-containing particles of 3-5 μm were confirmed. It could be observed that U and Pu are distributed at the same position in relatively densely packed particles that could be confirmed by secondary electron image (SEI). In Unit 3, a U-rich region attached to organic particles of about 10 μm was found. In the particles, U, Pu, and Zr appeared to adhere to different locations of the coarse particles.

Figure 11 shows a TEM image of U-containing particles in the Unit 2 stagnant water filtrate. The results of electron diffraction and elemental analysis showed that the particles were all cubic UO_2 containing Zr, Fe, Cr, or Zr.

Since most of the α-contaminant sources in the stagnant water were present in the form of particles, and the TEM observation of Unit 2 confirmed that U was chemically stable in the form of UO_2, the possibility of properties change over time was considered to be small.

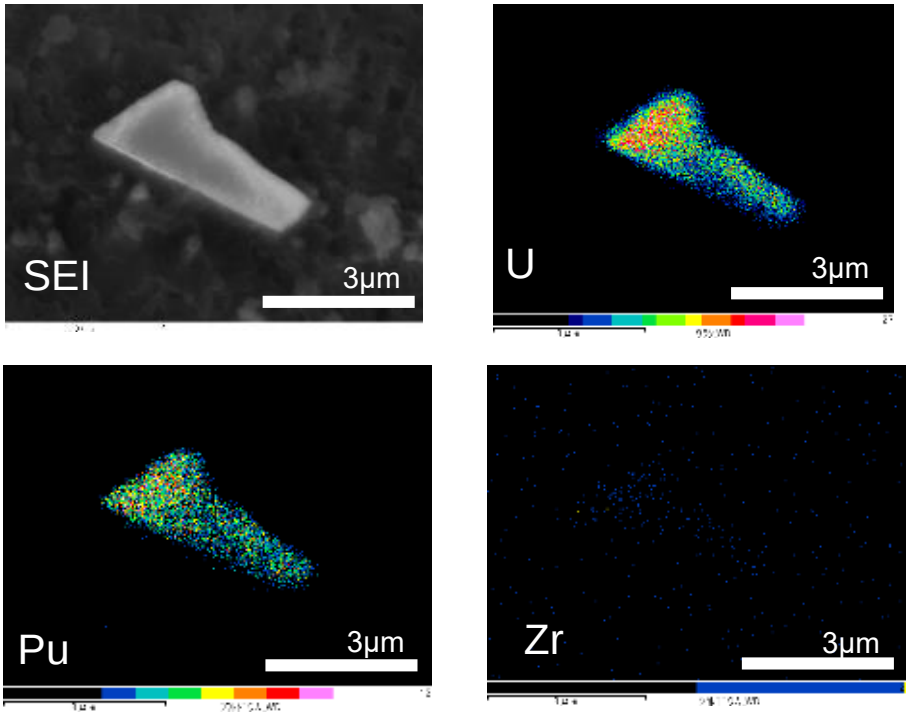

Figure 9 SEM-WDS results (Unit 2 torus room stagnant water filtrate)

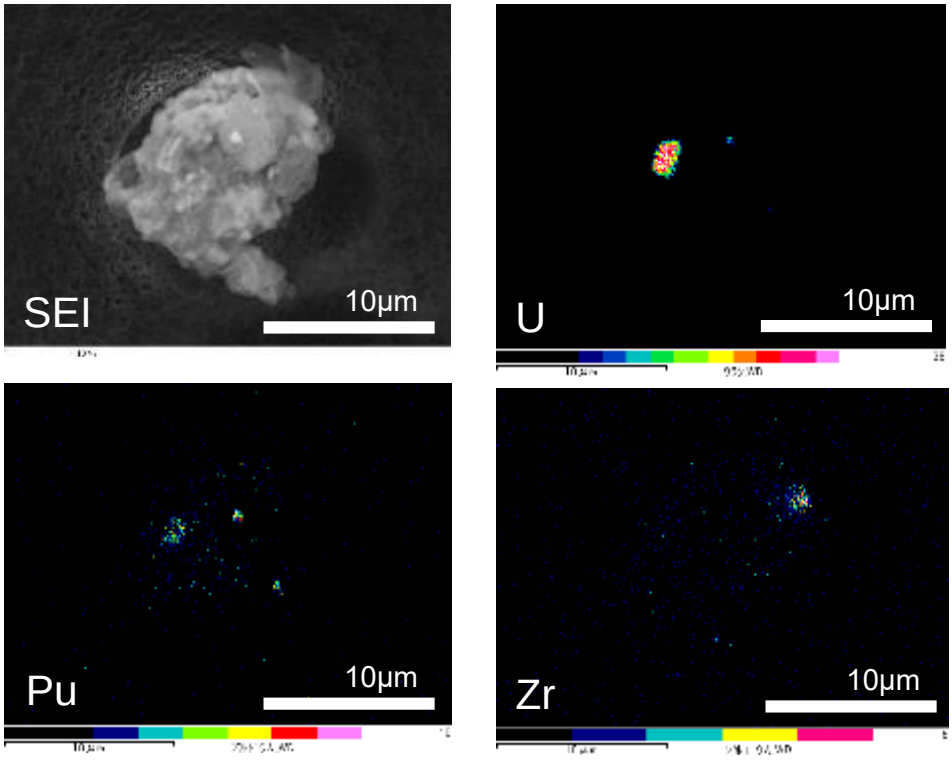

Figure 10 SEM-WDS results (Unit 3 torus room stagnant water filtrate)

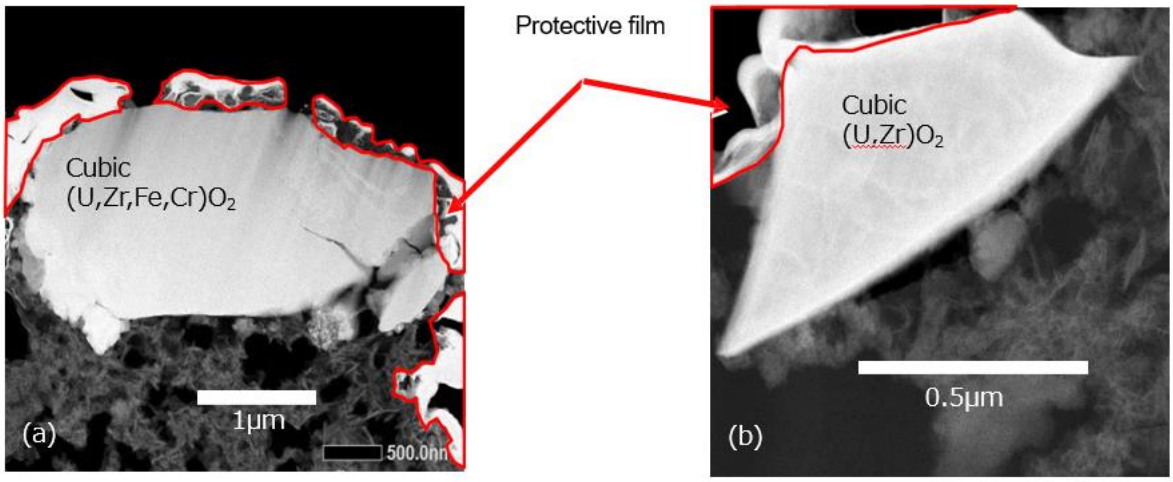

Figure 11　Results of TEM analysis

■　3.2 Evaluation of U isotope ratio distribution

The U isotope ratio ($^{235}U/(^{235}U+^{238}U)$) in the fuel is intentionally spatially distributed in the fresh fuel stage. The distribution of isotope ratios also depends on the results of the burnup during reactor power operation. The U isotope ratio is an important indicator for examining criticality, etc., and can also be an indicator of the degree to which U was mixed in with the progress of the accident. Therefore, isotope ratios were obtained by ICP-MS.

Figure 12 is a graph showing the U isotope ratio calculated from the ICP-MS analysis results of the contaminant samples obtained at Units 1 to 3. In the figure, samples in which a region with a high U concentration was found by SEM-EDS or WDS analysis are indicated by ○, and samples in which a region was not found by SEM-EDS or WDS are indicated by **X**. For comparison purposes, the natural U isotope ratio and the core average U isotope ratio of Units 1 to 3 calculated using the analysis code are also shown.

For the samples where regions of high U concentrations were found, many of them were close to the average value from the analysis code. In addition, some samples were found to be near the natural isotope ratios. Since diffusion and melt mixing due to high temperatures occur during an accident, the range of the U isotopic ratio distribution of the products is expected to be smaller, and this may cause many of the samples to be near the average value.

On the other hand, for the samples where no regions of high U concentration were found, the width of the distribution was larger than for the samples where they were found, ranging from near the value for natural U to just over 3%. This could be due to the analytical precision for the low U content to the extent that no U-enriched regions were found by SEM-EDS/WDS, possible local effects, etc.

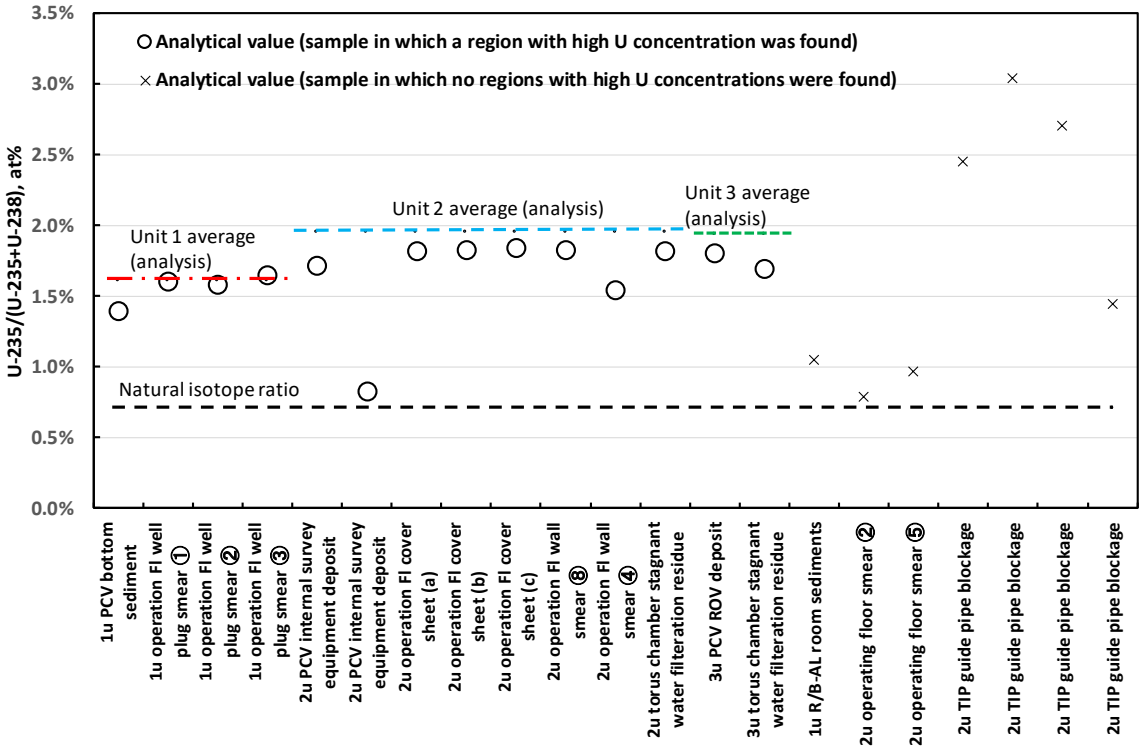

Figure 12　U isotope ratios obtained from ICP-MS analysis results

■　3.3 Evaluation of U-containing particle formation process

In this and the following sections, mainly the results of observations of radioactive particles containing U, etc. and an evaluation focusing on the particle formation process are presented.

Figure 13 shows an image of the formation process of U-containing particles. Most of the U in the fuel melted down to form fuel debris mixed with structural materials and was present in the reactor and containment vessel, but a part of the debris became fine particles and moved with the flow of gases such as steam and hydrogen and the flow of liquids such as water. The formation process of such U particulates can be roughly divided into two types: one is by melting and solidification, and the other is by evaporation and condensation.

The fuel rods that make up the fuel assembly are composed of UO_2 pellets, which are a nuclear fuel material, in a Zr alloy (Zircaloy) cladding tube. Therefore, the reaction of Zr as well as U is important during the period when U is melting or evaporating and migrating. When dissimilar materials react, melt, and solidify, the products are considered to contain the constituent elements of each material. On the other hand, when the products are formed by evaporation and reaction in the gas phase, they may have characteristic compositions such as being separated by vapor pressure differences.

Based on the above, an attempt was made to classify the particles based on the composition (content of Zr, etc.) and shape of the particles obtained from the analytical results, according to whether they underwent processes ① or ② given below.

① Melting and solidification process

The particles containing Zr were basically classified as particles formed by the melt-solidification process. Particles might have fracture surfaces associated with crushing.

② Evaporation and condensation process

In the presence of sufficient water vapor, the vapor pressure of Zr oxides is much lower than that of other oxides, therefore the Zr-free particles were basically classified as particles formed by the evaporation-condensation process. In some cases, fine particles aggregated and had a nearly spherical shape.

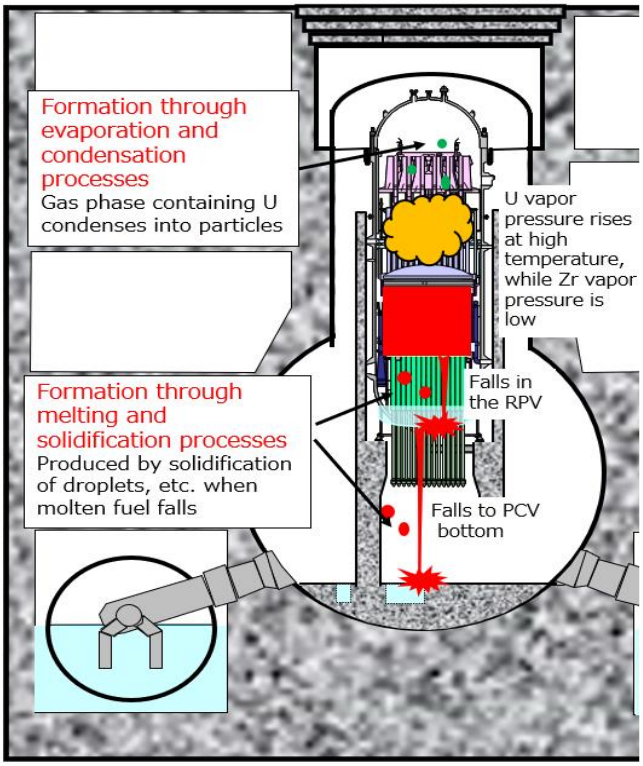

Figure 13 Image of U-containing particle formation process

■ 3.4. U-containing particles containing α-Zr(O) phase

As the results of TEM analysis of U-bearing particles detected in the bottom sediment of the Unit 1 PCV, Figure 14 shows a Z-contrast image, Figure 15 shows EDS mappings for U and Zr, and Figure 16 shows elemental analysis results (point analysis). The particles had an angular outer shape of about 2 μm. EDS mappings showed that regions of high Zr concentration were scattered among regions of high U concentration. From the results of electron beam diffraction and elemental analysis, the regions with high U concentration including analysis points ①, ③, ④, and ⑤ were considered to be the $(U,Zr)O_2$ phase, and analysis point ② in the region with high Zr concentration was $(U,Zr)O_2$ and α-Zr(O) was presumed to coexist.

Based on the above analysis results, the process by which the U-containing particles were formed was examined. Based on the presence of $(U,Zr)O_2$ phase, the coexistence of U and Zr,

and the angular shape, it was presumed to have been formed by the melting and solidification process. α-Zr(O) observed in the $(U,Zr)O_2$ phase was considered to have precipitated in the matrix phase ($(U,Zr)O_2$ phase) during the solidification process of high-temperature molten U-Zr-O. If there is a lot of water vapor when the particles solidify, Zr might also be oxidized to form ZrO_2, and it is possible that there was a relatively large amount of hydrogen before the particles solidified.

Figure 17 shows an image of the precipitation process of α-Zr(O) observed in the $(U,Zr)O_2$ phase described above on the pseudo-binary phase diagram of α-Zr(O) and UO_2 [7]. The liquid phase of U-Zr-O (one or two phases coexisting) melted at a high temperature precipitates as a solid $(U,Zr)O_{2-x}$, which has a relatively high melting point, when cooled below about 2400℃. Upon further cooling, α-Zr(O) precipitates below about 1900° C and coexists with $(U,Zr)O_{2-x}$. Although it is necessary to refer to the ternary state diagram of the U-Zr-O system for a detailed and rigorous discussion, including composition, the pseudo-binary phase diagram was used here for a simpler explanation.

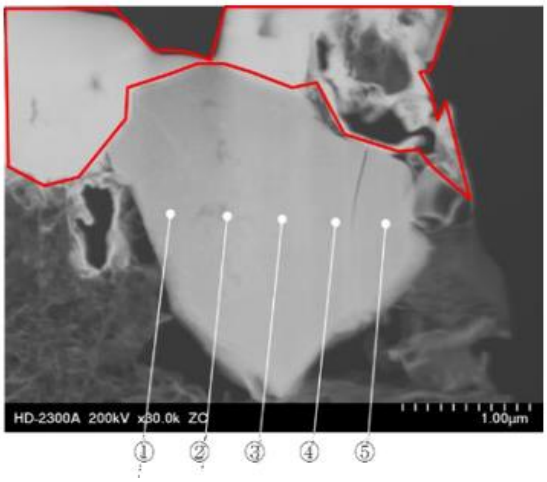

Figure 14　TEM analysis result: Z-contrast image
(The area enclosed by the red frame is the protective layer.)

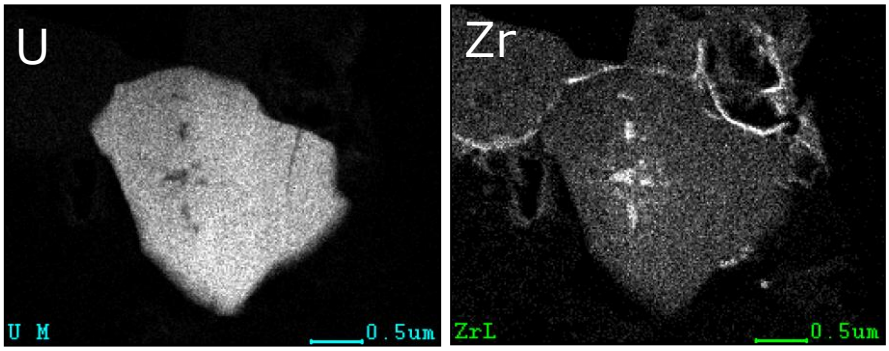

Figure 15　TEM-EDS mappings

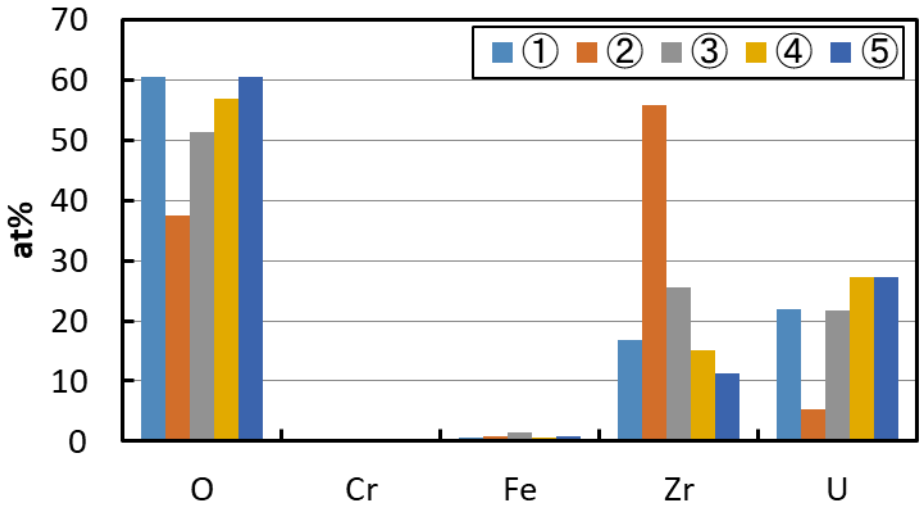

Figure 16　Elemental point analysis

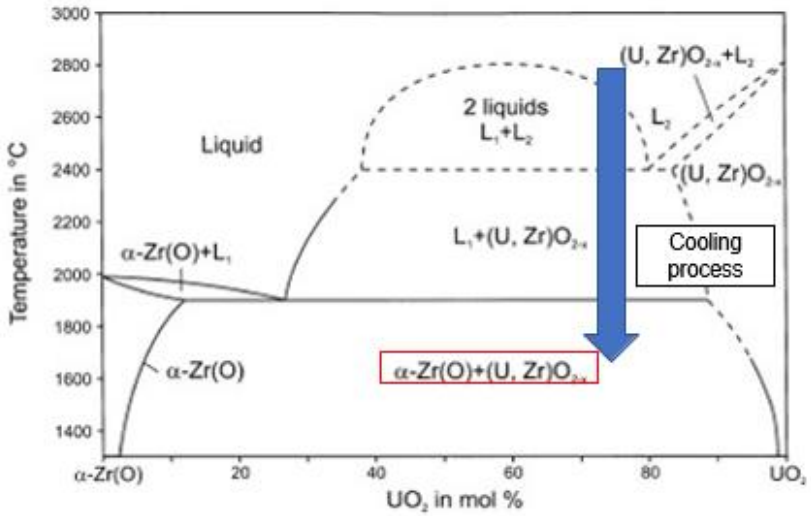

Figure 17　α-Zr(O)-UO_2 pseudo-binary phase diagram [7]
(With additional information)

■　3.5.　Fine particles containing monoclinic ZrO_2 phase

Figure 18 shows the Z-contrast image of a U-containing particle containing the monoclinic ZrO_2 phase detected in the Unit 1 PCV penetration (X-2) sediment sample; Figure 19 shows the EDS mapping results of U and Zr; and Figure 20 shows the point analysis results. Based on the results of electron beam diffraction and other analyses, the parent phase (region including points ① to ③ in Figure 18) was estimated to be cubic (U, Fe, Cr) O_2, and ④ was estimated to be monoclinic ZrO_2.

Since this particle contains Zr, it was estimated to have been formed by the melting and solidification process. Cubic (U,Fe,Cr)O_2 and monoclinic ZrO_2 shown in ④ coexist in this

particle, and considering that they were formed by phase separation, the following process can be considered based on the ZrO2-UO_2 pseudo-binary phase diagram [8] in Figure 21. First, U-Zr-O in the liquid phase at high temperature changes to cubic $(U,Zr)O_2$ upon cooling. A subsequent cooling process is considered to have separated the cubic $(U,Zr)O_2$ into cubic $(U,Zr)O_2$ and tetragonal $(Zr,U)O_2$. Subsequently, the tetragonal crystal is considered to have changed to monoclinic ZrO_2.

The cooling rate is considered to have been slow enough to cause the separation of cubic $(U,Zr)O_2$ and tetragonal $(Zr,U)O_2$, which may be related to the large heat of the fuel debris that fell in Unit 1 and the fact that water injection was not performed for a long time.

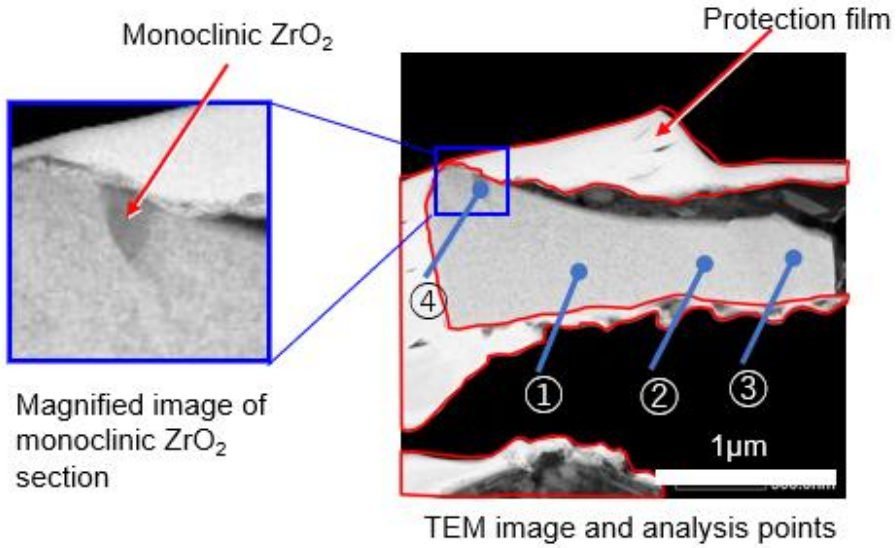

Figure 18 Z-contrast image
(Particles of sediment in PCV penetration (X-2) in Unit 1)

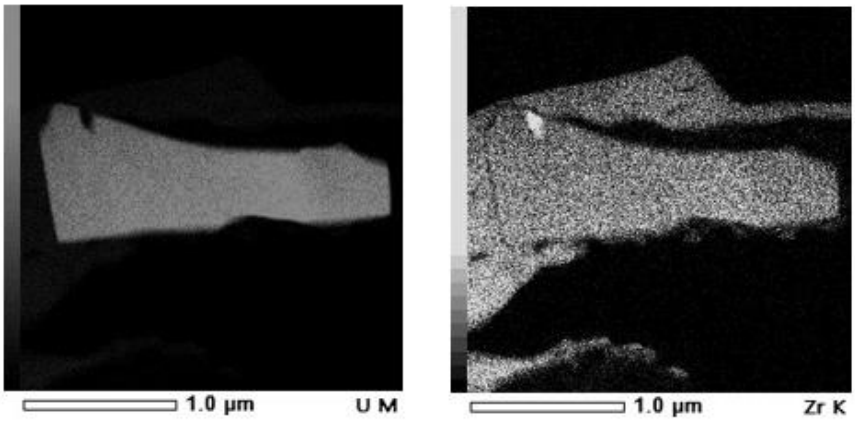

Figure 19 EDS mapping
(Particles of sediment in Unit 1 PCV penetration (X-2))

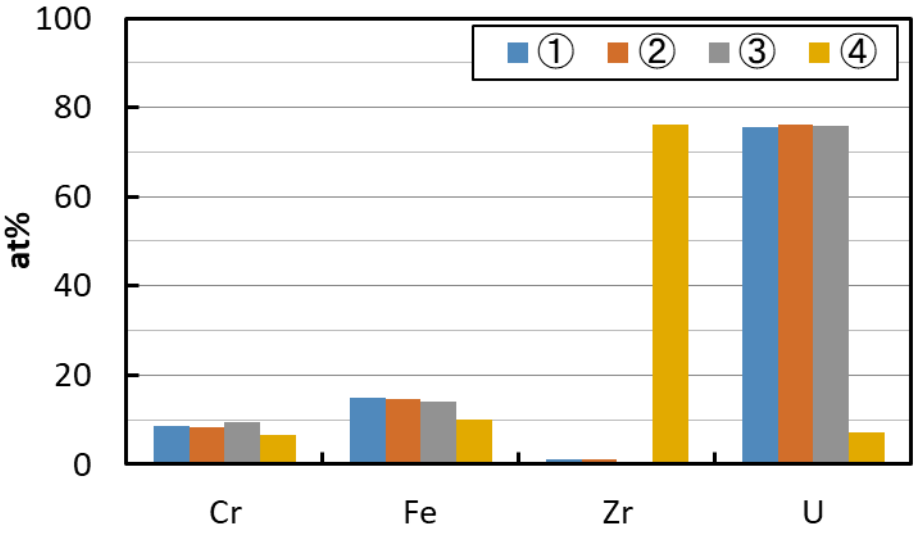

Figure 20 Point analysis results

(Micro particles in the PCV penetration (X-2) of Unit 1)

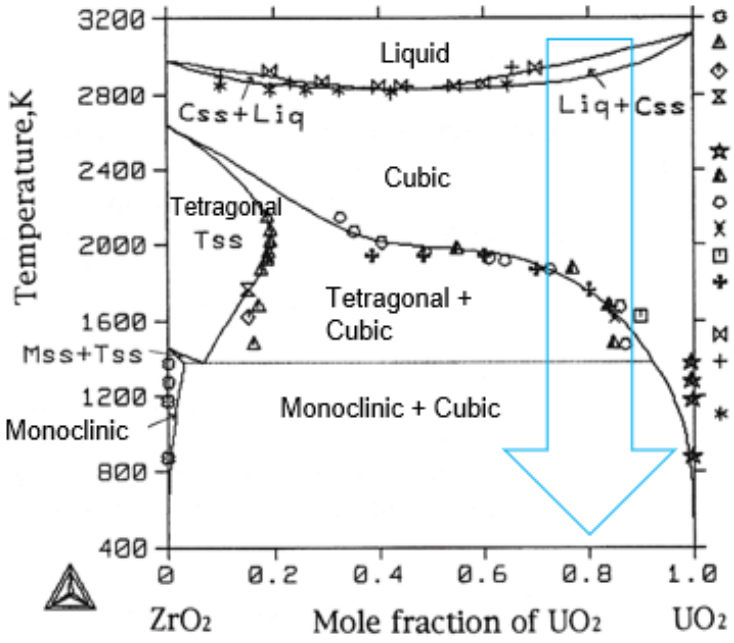

Figure 21 ZrO_2-UO_2 pseudo-binary phase diagram [8]

(With additional information)

■ 3.6. Multi-component particles with fuel rod and steel components fused together

On the Unit 2 operating floor, particles were found in which steel components (Fe, Cr) and fuel rod components (U, Zr) were fused together. Figure 22 shows a TEM image. The results of electron diffraction and elemental analysis show that the particles consist of a mixed phase of cubic (U,Zr,Fe,Cr)O_2, which appears as white in the TEM image, and the gray area is $FeCr_2O_4$.

Since these particles contain Zr, they are considered to have been produced in the process of melting and solidification. Further, it is characteristic that cubic (U, Zr, Fe, Cr)O_2 and $FeCr_2O_4$ are intricately mixed in a region of several tens of nm. This is thought to be due to phase separation during the cooling process of the U-Zr-Fe-Cr-O system melt, and it is consistent with the existing knowledge that the fuel involved the steel material and formed fuel debris.

Since the precipitate size depends on the cooling rate, if the relationship between the precipitate size and the cooling rate is clarified by tests, etc., it may be useful for estimating the cooling rate during particle formation.

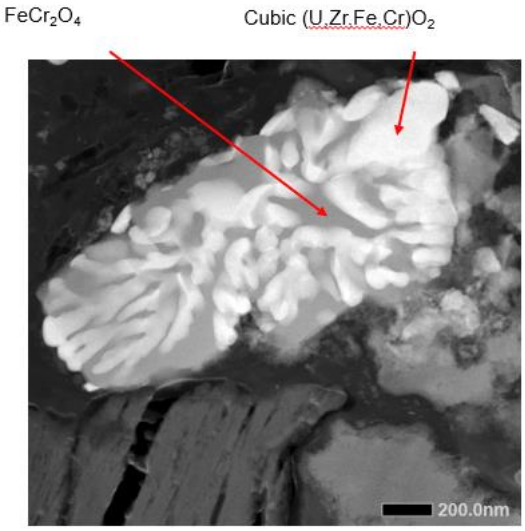

Figure 22 TEM analysis results
(Particles that appear to be fused with fuel rod and steel components)

■ 3.7. Particles formed by the evaporation and condensation process

In the analysis of contaminated material samples, in addition to particles presumed to have undergone the melting and solidification process, particles presumed to have undergone the evaporation and condensation process were also identified. Figure 23 presents TEM images of particles found on the Unit 2 reactor building operating floor. All particles are a few μm in diameter and round shape, and they contain U with a little Zr, so they were assumed to have undergone an evaporation-condensation process. The particle in A is spherical overall, but when looking at it closely, it has an agglomerated structure of U oxide particles with a diameter of about 100 nm, and Fe oxides are present in the gaps between them. The particle in B is a spherical particle with a relatively dense microstructure compared to the particle in A.

There are also Fe oxides that appear dark gray around the spherical U-containing particles.

Based on the above observations, particles in A and B may have been formed by the following process. The high temperature at the time of the accident increased the vapor pressure of the U component in the fuel, causing some of it to evaporate, but it immediately solidified to form small particles of UO_2. These small particles are considered to have agglomerated while entrapping Fe oxides and other substances. Subsequently, the agglomerated particles are assumed to have grown into crystals while the Fe oxides are swept away as seen in particle in B.

The particle in C (cubic UO_2) can be considered as an intermediate state between particles in A and B in terms of crystal growth, but they differ in that there are amorphous SiO_2 particles in the vicinity of the cubic UO_2 crescent-shaped particles. The shape of the particle in C suggests that cubic UO_2 deposited on the surface of spherical particles of amorphous SiO_2 may have been separated and formed later.

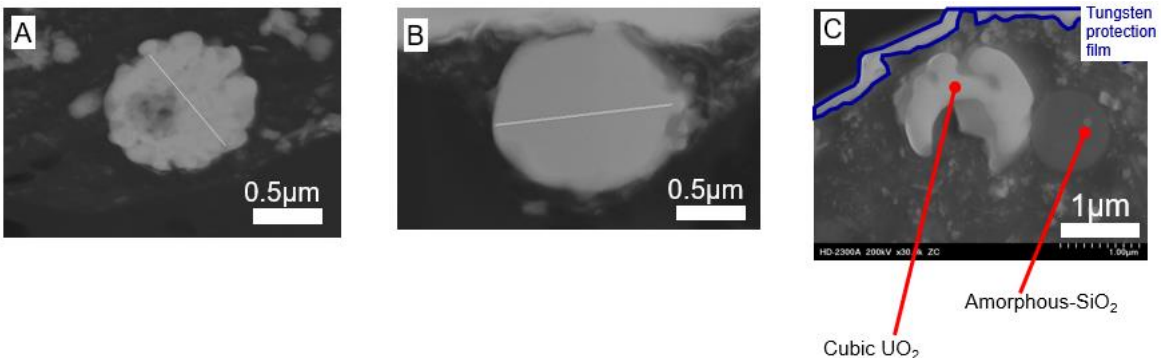

Figure 23　Particles estimated to have undergone the evaporation and condensation process

■　3.8.　Fine particles mainly composed of iron

In addition to the information given by U and Zr, which are fuel constituents, there is a possibility that information on accident progression can be extracted through analysis focusing on iron, which is a constituent of core internals.

Figure 24 shows iron-based spherical particles containing a small amount of U found on the curing sheet on the Unit 2 operating floor. From the results of TEM-EDS and electron diffraction, it was found that body-centered cubic pure Fe and spinel-structured Fe_3O_4 are present adjacent to each other.

The particles are believed to have undergone melting due to their spherical shape. In this case, it is considered that the liquid phase Fe–O melted at a high temperature was cooled to become the FeO solid phase, and phase separation into Fe and Fe_3O_4 occurred in the course of further cooling. Referring to the oxygen potential-temperature relationship of the Fe–O system shown in Figure 25, the FeO solid phase can be formed during solidification when the partial pressure ratio $p(H_2)/p(H_2O)$ of hydrogen and water vapor is in the range of 0.02 to 1. Strictly speaking, it is necessary to consider the influence of impurities, etc., but it is thought that the atmosphere in which the partial pressure of water vapor was higher than the partial

pressure of hydrogen during solidification, and the conditions inside the reactor during the formation of these particles were not those of a completely hydrogen-filled environment and were thought to be rich in water vapor.

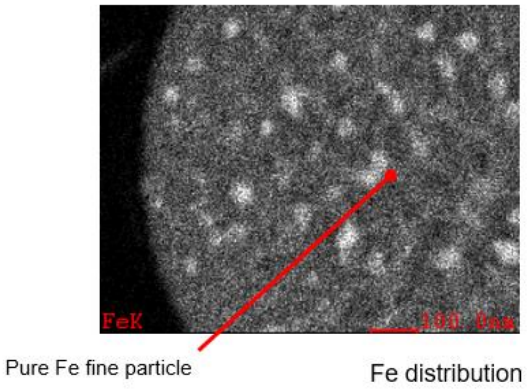

Figure 24　Particles mainly composed of iron

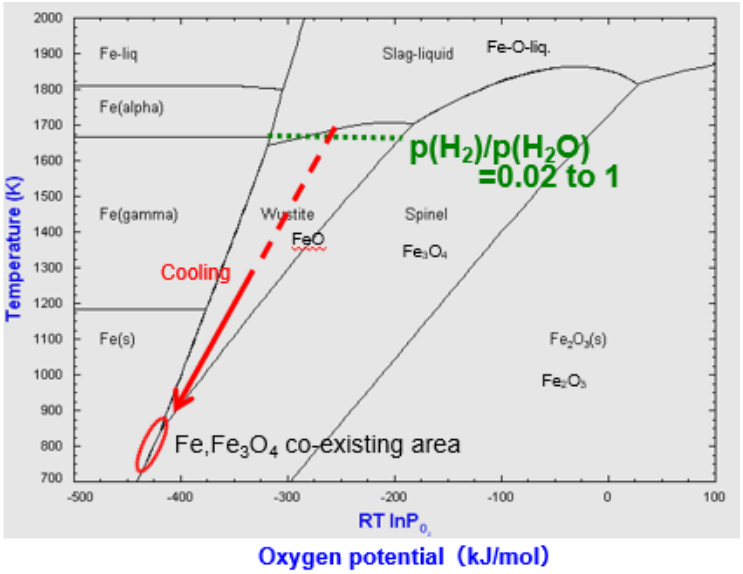

Figure 25　Oxygen potential-temperature diagram of Fe-O system

■　3.9. Study on insoluble Cs particles in the environment

Insoluble spherical Cs particles (Type A) with a size of 1-10 μm containing radioactive Cs and containing amorphous SiO_2 as the base material have been found outside the power station site (Figure 26). Similar spherical Si particles with low Cs concentration have also been found in samples collected on the Unit 2 operating floor (Figure 27). Insoluble Cs particles (Type A) were formed at the time of the accident, as well as U-containing particles, and it is thought that investigating the formation process of these particles will be useful in examining the progression of the accident. Considering the meteorological conditions at that time and the origin of the constituent elements, the insoluble Cs particles (Type A) are believed to have originated in Unit 2.

The reactor pressure and containment pressure of Unit 2 are shown in Figure 28. Based on the accident progression, it is considered that Si and Cs reacted in the RPV to form particles, which migrated to the PCV at the timing of the PCV pressure increase and were released into the environment while going through a rapid cooling process. At a certain high temperature, Mo is released from the fuel. In this situation, the affinity between Cs and Mo is high, and the SiO_2 particles produced would not contain Cs. Therefore, the temperature and atmosphere conditions when the particles migrated to the PCV may have been above the SiO_2 liquefaction temperature, above the Cs release temperature from the fuel, and below the Mo release temperature (depending on the atmosphere), that is, in the temperature range of 1500 to 2300°C with high hydrogen content (for details, see Appendix 5, Appendix 1).

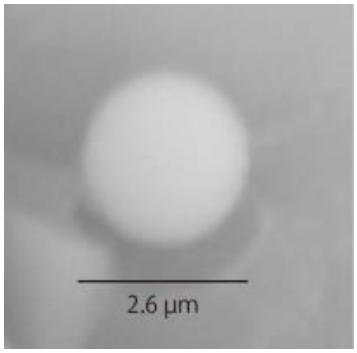

Figure 26　Insoluble Cs particles (Type A) [9]

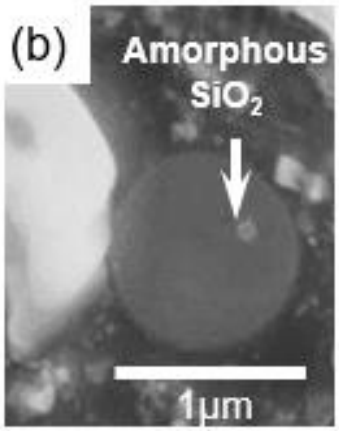

Figure 27　Amorphous SiO_2 particles collected on the Unit 2 operating floor

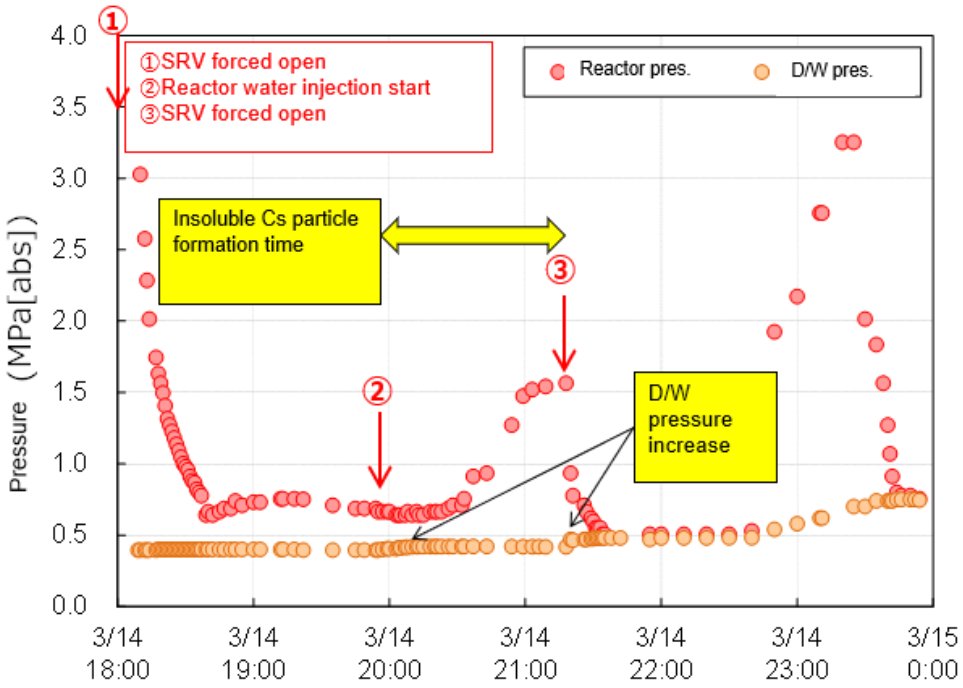

Fig 28 Reactor pressure and containment pressure of Unit 2

■ 4. Summary

Based on the analysis results of samples from the 1F site and reports of insoluble Cs particles observed in the environment, a study was conducted to extract information useful for understanding the state of fuel debris and the accident progression. As a result, the following findings were obtained.

<Findings on the state of fuel debris>

- Most of the alpha contamination sources in stagnant water were present in the form of particles, and more than 90% of them could be removed with filter paper. U is chemically stable in the form of cubic UO_2 and is unlikely to change over time.
- Based on the analysis results of the U isotope ratio (^{235}U/total U) in the sample, it was believed that the mixing of U isotopes progressed due to fuel melting.

<Findings related to the progression of the accident (from the evaluation of the formation process of radioactive fine particles)>

The results suggested that the chemical environment (hydrogen/water vapor ratio, etc.) inside the RPV/PCV changed with time and place.

- In Unit 1, particles thought to have been formed in a hydrogen-rich environment were confirmed, and these particles might be related to insufficient water injection into the reactor in the early stages of the accident.
- In Unit 2, particles thought to have been formed in an environment with a lot of water vapor and particles thought to have been formed in an environment with a lot of hydrogen were confirmed. The timing of formation of insoluble Cs particles was

considered to be the initial stage of the fuel temperature rise and was thought to be a clue to the environment inside the RPV at the time of their formation.

■ 5. References

[1] TEPCO “56th Decommissioning and Contaminated Water Response Team Joint Meeting, Document 3-3, Preparation for fuel debris retrieval, Analysis results of samples related to investigation inside Units 1 to 3 reactor containment vessels”, https://www.tepco.co.jp/decommission/information/committee/roadmap_progress/pdf/2018/d180726_08-j.pdf (July 26, 2018)

[2] TEPCO “66th Decommissioning and Contaminated Water Response Team Joint Meeting, Document 3-3, Preparation for fuel debris retrieval, Analysis results of samples related to investigation inside Units 1 to 3 reactor containment vessels”, https://www.tepco.co.jp/decommission/information/committee/roadmap_progress/pdf/2019/d190530_07-j.pdf (May 30, 2019)

[3] TEPCO “66th Decommissioning and Contaminated Water Response Team Joint Meeting, Document 3-3, Preparation for fuel debris retrieval, Analysis results of samples related to investigation inside Units 1 to 3 reactor containment vessels”, https://www.tepco.co.jp/decommission/information/committee/roadmap_progress/pdf/2020/d201126_08-j.pdf (November 26, 2020)

[4] TEPCO “101th Decommissioning, Contaminated and Treated Water Response Team Joint Meeting, Document 3-3, Preparation for fuel debris removal, Analysis of samples obtained at Fukushima Daiichi Nuclear Power Plant", https://www.tepco.co.jp/decommission/information/committee/roadmap_progress/pdf/2022/d220427_08-j.pdf (April 27, 2022)

[5] TEPCO/JAEA「debrisWiki」https://fdada-plus.info/wiki/

[6] A. Nakayoshi et al, "Analysis of in-vessel deposits at Fukushima Daiichi Nuclear Power Plant in FY 2009 and 2018; Subsidy for Decommissioning and Contaminated Water Countermeasure Project" (Development of technology for understanding and analyzing properties of fuel debris), https://doi.org/10.11484 /jaea-data-code-2021-011, JAEA (2022)

[7] A. Skokan, High-temperature phase relations in the U-Zr-0 system, 5th Int. Meeting on Thermal Nuclear Reactor Safety, Karlsruhe, FRG (1984).

[8] M. Yamashita, et al., J. Amer. Ceramic Soc., 79 (1996) 521.

[9] K. Adachi, et al. "Emission of spherical cesium-bearing particles from an early stage of the Fukushima nuclear accident." Scientific Reports 3.1 (2013): 1-5.

Phenomenological study on the formation mechanism of insoluble cesium particles type A

This material was initially prepared for submission for separate publication. However, since the discussion leads to information that can be applied to understand the behavior of FPs during accidents from known information, it was deemed appropriate to summarize it as this document.

■ 1. Introduction

After the Fukushima Daiichi Nuclear Power Station accident in 2011, particles containing radioactive cesium were widely discovered in the Fukushima area and the metropolitan Tokyo area, and their compositions and structures have been reported by environmental scientists [1]-[10]. These particles are broadly classified into two types, Type A and Type B. Type A is characterized as having a relatively spherical shape, high specific activity, and a glassy SiO_2 base with a diameter of approximately 1-10 μm as a matrix, while Type B is characterized as having a relatively low specific activity and consisting of large particles with a non-spherical shape of several hundred μm [3].

Type B is evaluated to have been formed from Unit 1 based on the $^{134}Cs/^{137}Cs$ ratio, etc., and to have been released during the reactor explosion based on its irregular shape and distribution area [3]. On the other hand, Type A is estimated to have been formed from Unit 2 or 3 based on the $^{134}Cs/^{137}Cs$ ratio and formed in the high-temperature region where SiO_2 melted, based on its spherical shape [3].

It is important to estimate the formation process of these insoluble Cs particles in order to evaluate their impact on the environment. The formation process has been proposed as an in-reactor pressure vessel process (In-RPV process), a molten core concrete interaction reaction process (MCCI process), and a filter fire process, but there is no clarification as to which process they went through. Plant information and analytical results of the inside of the particles are important in studying the formation process of insoluble Cs particles (analytical results of the particle surface do not show the true information of the particles because they emphasize information such as attached elements and contamination on the surface).

Of the three formation processes described above, a formation process due to a filter fire in the emergency gas treatment system (SGTS: standby gas treatment system) has been reported [11]. However, an on-site investigation of the SGTS filter train confirmed the absence of damage [12], and this hypothesis was clearly rejected. That is, the insoluble Cs particles are considered to be formed by either the In-RPV process or the MCCI process. If formed by

the MCCI process, SiO_2 is considered to originate from concrete, and given its spherical shape, it is reasonable to assume that the melt solidified, and the change in constituent elements during the transfer of the concrete melt to the gas phase is considered to be small. Therefore, if the MCCI process is assumed, insoluble Cs particles should contain a considerable amount of concrete constituent elements such as Ca and Al. In the case of the In-RPV process, on the other hand, these elements are considered to be almost absent because there are no components containing these elements in the reactor.

Reported values [4], [5] for the composition of Type A insoluble Cs particles are given in Table 1. The compositions are almost equal, with about 70 wt% silica base containing about 10 wt% zinc and iron oxides, 3-10 wt% cesium oxides, and 1-3 wt% tin oxides, rubidium oxides, potassium oxides, and chlorine. On the other hand, the amount of Ca and Al relative to SiO_2 is clearly lower than the composition in the concrete, with only a few samples showing almost no or very small amounts of Ca and Al, which are found in Type B. This probably indicates that the origins of Type A and Type B silica are different, but their origins are not clear. In other words, knowing the origins of Zn, K, and Cl, as well as Si, whose origin is not clear, is expected to be useful in narrowing down the location and conditions for the formation of insoluble Cs particles and it is considered important in the investigation of their formation mechanism.

In this appendix, focus is put on the formation mechanism of spherical insoluble Cs particles classified as Type A among the insoluble Cs particles in the Fukushima Daiichi Nuclear Power Station accident, and the formation location and formation process are evaluated by comparing the composition of the reported particles with the formation elements based on plant information such as elements present in the area where the particles are assumed to have formed, and the amount of particles formed in that process during the accident.

■ 2. Phenomenological consideration of formation mechanism

■ 2.1 In-RPV process vs. MCCI process

Since the insoluble Cs particles are based on glassy silica, the process of silica glass sphere formation is examined. There are two possible mechanisms by which silicon evaporates at high temperatures and silica glass spheres are assumed to form. One is the mechanism of formation in the RPV (In-RPV process), and the other is due to MCCI (MCCI process). Here, the information for samples with clear sample capture times can be summarized as follows.

1) The time of insoluble Cs particle capture at Tsukuba was from 21:10 on March 14, 2011 to 09:10 on March 15, 2011, and from 00:00 to 16:00 on March 15 at Setagaya-

ku, Tokyo. The particles are evaluated as having been released on the night of March 14 [1],[10].

2) The start of the fuel melt in Unit 2 is evaluated to have occurred on the night of March 14 (see Attachment 2-4 and Attachment 3).

3) Based on the change in the CAMS indicator value of the drywell (D/W) in Unit 3, it is possible that the fuel in Unit 3 had fallen into the containment vessel at 04:10 on March 14.

Therefore, insoluble Cs particles are considered to have been formed in Unit 2 by the In-RPV process and in Unit 3 by the MCCI process. Table 2 summarizes the main findings of the environmental studies and the gaps in these findings for each assumed mechanism (In-RPV process and MCCI process). In order to validate the assumptions regarding these formation processes, it is necessary to examine the presence/absence of elements and compounds in each mechanism, as described in the following sections.

■ 2.2 Considerations on elements of unclear origin

Type A insoluble Cs particles consist of a SiO_2 glass matrix of about 70 wt%-SiO_2 and contain no other natural mineral elements such as Al or Ca, as shown in Table 1. Assuming that concrete is the origin of Si, it is difficult to explain the mechanism of loss of Ca and other elements from the particles during the concentration process in the evaporation-condensation or MCCI process, as shown in Section 3, and the same is presumed for Al. On the other hand, if Si is assumed to originate from Si (containing less than 1 wt%) added into SUS (stainless steel), it is necessary to assume a geometric configuration that heats up to a temperature higher than the melting point of SUS and other materials because of the low vapor pressure of Si.

Table 1 Composition of insoluble Cs particles of Type A

unit: wt%

	Yamaguchi, et al.		Kogure, et al.				
	NWC-1	CB-8	P6-6 (ave.)	G3-8 (ave.)	W-01 (ave.)	P6-6 (Center)	P6-6 (Cs-max)
SiO_2	69.3	73.3	72.7	64.8	61.3	80.5	65.9
Cl	1.4	0.7	0.5	1.1	1.0	0.3	0.7
K_2O	1.9	1.4	1.2	1.2	0.8	1.6	0.7
Fe_2O_3	8.6	7.2	7.2	7.8	9.1	6.6	7.5
ZnO	11.0	11.4	7.9	12.0	12.0	6.7	9.0
Rb_2O	1.3	1.2	1.4	1.4	1.2	1.4	1.0
SnO_2	1.4	1.5	2.0	3.3	3.0	1.3	2.8
Cs_2O	3.4	3.3	7.2	8.5	11.7	1.6	12.4

(Normalized to 100% of the sum of the elements except oxygen)

	Yamaguchi, et al.		Kogure, et al.				
	NWC-1	CB-8	P6-6 (ave.)	G3-8 (ave.)	W-01 (ave.)	P6-6 (Center)	P6-6 (Cs-max)
Si	75.7	78.9	79.8	73.0	70.7	84.7	75.5
Cl	2.6	1.3	0.9	2.1	2.0	0.5	1.4
K	2.6	1.9	1.7	1.7	1.2	2.1	1.0
Fe	7.1	5.8	5.9	6.6	7.9	5.2	6.5
Zn	8.9	9.1	6.4	10.0	10.2	5.2	7.6
Rb	0.9	0.8	1.0	1.0	0.9	0.9	0.7
Sn	0.6	0.6	0.9	1.5	1.4	0.5	1.3
Cs	1.6	1.5	3.4	4.1	5.8	0.7	6.1

With regard to zinc, no zinc was injected into the cooling water at 1F, and no zinc-containing alloys were used in the fuel or core components. Therefore, it is difficult to explain the presence of zinc in the In-RPV process solely from zinc sources during normal operation. On the other hand, zinc-coated carbon steel is used for the inner grating of the RPV pedestal inside the PCV. This could be a possible basis for the case caused by the MCCI process.

Furthermore, it is inexplicable that Type A particles contain K and Cl. These elements are not normally present in reactor material designs. Although it cannot be ruled out that these could be due to seawater injection, the absence of Na and Mg suggests that the effect of seawater injection is small.

Table 2 Inexplicable items regarding assumed mechanism and composition/structure

Main findings from environmental research		Assumed mechanism (Unknown points regarding material chemistry)	
		High temperature gas phase reaction (Unit 2 RPV)	Molten core concrete reaction (Unit 3 MCCI)
Status of particle observation		Capture time in metropolitan Tokyo area (3/14 21:10-3/15 09:10 in Tsukuba) corresponds to Unit 2 nighttime emission event of 3/14	Cs-containing particles were confirmed in Unit 3 operation floor dust filter investigation (unconfirmed whether they are insoluble Cs particles)
Characteristics	Main composition is SiO_2 (SiO_2: about 70wt%)	・ Is the origin of SiO_2 a steel additive? ・ Low vapor pressure at steel melting point	・Is the origin of SiO_2 concrete? ・Reason why there is no Al or Ca?

of composition and structure	High Zn content (ZnO: about 10wt%)	・No Zn injection in cooling water ・Possible zinc coating	・Possibility of hot dip galvanizing of grating
	Fe content, no Cr (Fe_2O_3: about 10 wt%)	・Possibility of corrosion products (CRUD)	・Possibility of grating base material (carbon steel)
	FP component content (Cs/Rb »Ba/Mo)	・How to explain FP composition	・Same as left
	Specific component content (K, Cl)	・If derived from seawater composition, what about Na?	・Same as left
	Absence of B?	・How to explain control material behavior (B_4C)	・Same as left
	Multi-component spherical glass	・Evaporation and solidification at high RPV temperatures	・Evaporation solidification at high temperature by MCCI
	$ZnFe_2O_4$ phase separation	・Phase separation suppression; rapid cooling? ・Timing of rapid cooling at S/C transition, etc.	・What is the cause of formation of nano-crystal $ZnFe_2O_4$?

■ 2.3. Formation of franklinite component

Among transmission electron microscopy (TEM) observations of Type A insoluble Cs particles in which Zn and Fe have been observed, there are reports showing an entirely glass structure [4] and the presence of a franklinite ($ZnFe_2O_4$) separated phase in the particles [6]. For these two different TEM observations, it is believed that there is a single formation process and the observed differences are caused by slight differences in temperature and cooling rates. There is also a report that a $ZnFe_2O_4$-separated phase appeared when particles with a completely glass structure were heated at 900°C [13] and another report that a $ZnFe_2O_4$-separated phase appeared due to electron beam damage in TEM observations [8], which suggests that the $ZnFe_2O_4$-separated phase may have appeared within the sample due to an increase in sample temperature during observation.

To confirm the separation behavior of $ZnFe_2O_4$, a sample prepared to have the same composition as the insoluble Cs particles of Type A was heated and melted in a Pt crucible, and the entire crucible was quenched by water cooling, and the results were observed by TEM [14],[15]. According to these observations, nanoprecipitates of $ZnFe_2O_4$ with a diameter of 10-50 nm were observed in the glassy matrix in the central part of the sample, which was

difficult to cool, as shown in Figure 1. A rapid cooling from high temperature is required such that high-pressure gas is released into the suppression chamber (S/C).

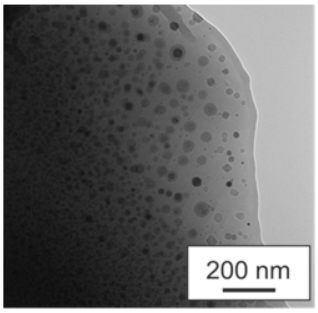

Figure 1 Franklinite precipitation test results in a simulated insoluble Cs particle sample [15]

■ 2.4. Inorganic zinc-containing paints

As mentioned above, particles with an entirely glass structure are thought to have formed in the RPVs with high temperature regions and were rapidly cooled by the opening of the SRVs, while no zinc-based materials were found in the RPVs, nor was zinc contained in the cooling water. Therefore, an investigation was made as to whether zinc-containing materials existed anywhere in the system leading to the RPVs, and it was found that paints with high inorganic zinc content in the construction records were applied to the inner walls of the suppression chambers (S/C) of 1F Units 1 through 3. The results of a 30-hour elution test at 140°C using zinc-containing paint coating samples shown in Table 3, which were prepared based on construction records [16], indicate that approximately 5 to 6 wt% Zn, 8 to 12 wt% Si, 15 to 25 wt% K, and 92 to 93 wt% Cl are eluted. Therefore, it is assumed that the above elements were deposited on the boiling surface in the RPV during RCIC operation in Unit 2, where the water source for the reactor core isolation cooling system (RCIC) was switched from the condensate storage tank (CST) to the S/C (unlike in other units). Assumption of this mechanism can explain the presence of the insoluble Type A Cs particles with constituent elements Si, Zn, K, and Cl.

Table 3 Composition and elution rate of simulated coating film containing zinc on the S/C inner surface

		Sample No.	Zn	Si	K	Mg	Ti	Al	Cl
Composition [15, 17] (wt%)	Before test	1	79	4.3	0.13	0.03	0.06	1.4	0.17
		2	78	4.0	0.16	0.03	0.07	1.6	0.13
	After test	1	74	3.8	0.11	0.01	0.05	1.4	0.012
		2	74	3.7	0.12	0.01	0.05	1.4	0.010
Elution rate (wt%)		1	6	12	15	67	17	0	93
		2	5	8	25	67	29	13	92
		ave.	6	10	20	67	23	6	93

■ 3. Examination of cesium chemistry

FPs are generally classified into four groups according to their evaporation properties [17],[18]. The first group consists of volatile FPs such as Xe, Kr, Cs, I, Te, Sb, Ag, Cd and Rb; the second group consists of semi volatile FPs such as Ba, Mo, Tc, Rh and Pd; the third group is low volatility FPs such as Ru, Ce, Sr, Y, Eu, Nb and La; the fourth group is non-volatile FPs such as Zr, Nd and Pr. This difference in evaporation behavior suggests that the vapor phase content in the RPV during particle formation was Cs>>Ba. On the other hand, Type A insoluble Cs particles contain Cs and Rb, but little or no Ba is present or it is below the TEM/EDS detection limit, and the FP content within Type A insoluble Cs particles is also Cs>>Ba. Thus, the composition within the insoluble Cs particles of Type A is consistent with the vapor phase content in the RPV. The release of Cs from the oxide fuel becomes significant from about 1500°C [18],[19], and the release of Ba requires a temperature of about 2300°C [18]. Thus, Type A insoluble Cs particles are considered to have formed in the Unit 2 RPV in the fuel temperature range of about 1500-2300°C. In this temperature range, there is also less release of Mo, which inhibits the formation of insoluble Cs particles by forming cesium molybdate that is thermodynamically more stable than cesium silicate.

It has been experimentally confirmed that the presence of Mo suppresses the formation of insoluble Cs particles; a simulated test method for understanding the formation mechanism of insoluble Cs particles using SiO_2 as a matrix material [14] was used to test the addition of a Mo evaporation source, and as shown in Figure 2(a), only a little Si containing Mo-Cs-O particles formed [14]. In the temperature range of 1500-2300°C in an atmosphere where Mo is in a metallic state, Cs is released from the oxide fuel but the Mo vapor pressure is low, Cs-Si-O is formed, and as the temperature increases further and the

Mo vapor pressure increases, the formation of Cs-Si-O is suppressed, or Cs-Si-O changes to Cs-Mo-O as the Mo vapor pressure increases. Experiments with Zn and Ca added to the evaporation source, assuming the influence of inorganic zinc-containing coatings and concrete as the source of Cs-Si-O, have shown the presence of Zn and Ca in Cs-Si-O particles, as seen in Figures 2(b) and 2(c) [14]. In other words, since Ca is not observed in the Type A insoluble Cs particles observed in the metropolitan Tokyo area, it is judged that the MCCI process, which contains Ca in the source, is unlikely as the formation mechanism of these particles.

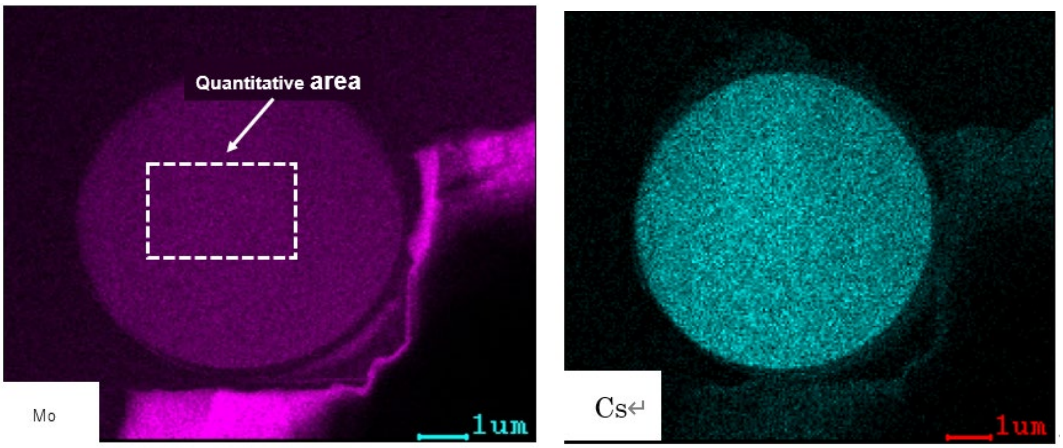

(a) Mo and Cs distributions on cross section of a formed Mo-Cs-O particle obtained by TEM (Mo, 46%; Cs, 53%; Si, 1%)

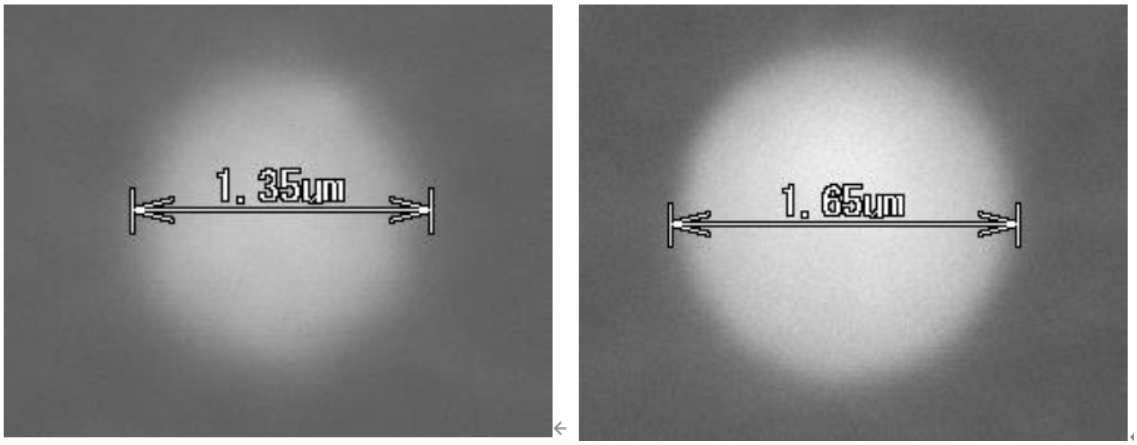

(b) SEM image of Zn containing Cs particle (Si, 56%; Cs, 17%; Zn, 22%)

(c) SEM image of Ca containing Cs particle (Si, 69%; Cs, 29%; Ca, 1%)

Figure 2 Effect of Mo, Zn and Ca on the formation of insoluble Cs particles [15] (Unit: at% metal element)

Another important element present in the reactor during an accident is B, which forms Cs-B-O [20] that is more thermodynamically stable than Cs-Si-O or Cs-Mo-O. With respect to B behavior, there are usually two processes. One is the melting process by the B_4C-SUS reaction in control rods [21], and the other is evaporation as HBO_2 formed by the B_4C-water vapor reaction after control rod melting. In the reducing atmosphere in the early stage of fuel melting, the B_4C-SUS reaction is considered to be dominant, and B is not involved in the formation of Cs-Si-O. On the other hand, when the steam atmosphere becomes stronger and evaporation by the B_4C-water vapor reaction is dominant, Cs-B-O forms and the formation of Cs-Si-O is suppressed.

Based on the above, it is judged that the Type A insoluble Cs particles observed in the metropolitan Tokyo area were most likely formed by the In-RPV process in the early stage of fuel melting in Unit 2.

■ 4. Estimation of material behavior in Unit 2

As mentioned above, it is highly likely that the Type A insoluble Cs particles observed in the metropolitan Tokyo area formed in the RPV of Unit 2. Therefore, the history of material behavior in Unit 2 is summarized below.

During normal operation, most of the Cs is retained in the fuel grains and some precipitates at grain boundaries. Iron CRUD is caused by corrosion of carbon steel piping and migration of corrosion products into the RPV by cooling water flow and precipitation on the cladding boiling surface.

After the 14:46 earthquake on March 11, 2011, the RCIC was still in operation and the CST was initially used as the cooling water supply source, but only Unit 2 switched from the CST to the S/C. It is also estimated that the S/C water temperature rose to approximately 140°C during RCIC operation in Unit 2. This is believed to have caused elements such as Si, Zn, K, and Cl to leach into the S/C water from the inorganic Zn-containing coating applied to the S/C inner wall, migrate with the cooling water to the RPV, and deposit on the cladding boiling surface.

The RCIC was shut down around 09:00 on March 14, and the RPV pressure began to rise. Subsequently, forced depressurization of the RPV took place at 18:00 on March 14, and core overheating began. Figure 3 shows the pressure measurement data after the forced depressurization of Unit 2. It is evaluated that the SRVs were forced open at (1) (18:02), water injection resumed at (4) (19:54), SRV closure occurred at (5) (around 20:15), in-core steam and hydrogen production occurred at (6) (around 20:15 to 21:20), and SRVs were forced open at (7) (around 21:20). Among these events, the period between 20:00 and 21:20 when the RPV and PCV pressures were increasing ((4)-(7)) is considered to be the formation

period of Type A insoluble Cs particles, and the following phenomena are presumed to have occurred.

- Cladding rupture due to internal fuel rod pressure or inter-material reactions (formation of release pathways for FPs such as Cs and Rb)
- Evaporation of Fe CRUD from the cladding (transfer of Fe source to the gas phase)
- Evaporation of coating film components deposited on the cladding surface from the cladding (transfer of Si, Zn, K, and Cl sources to the gas phase)
- Evaporation of cladding components (transfer of Sn source to gas phase)
- Release of volatile FPs (transfer of Cs and Rb sources to the gas phase)
- Reaction and condensation of multi-vapor phase, densification of Cs-containing liquid phase with SiO_2 glass matrix (formation of completely glass micro-particles)
- Release of fine particles into the S/C with a large amount of water vapor and non-condensable gas at the SRV opening around 21:20 on March 14 (rapid cooling of fine particles by transfer from the high-temperature gas phase in the RPV to the low-temperature water phase in S/C in a few seconds)

Type A insoluble Cs particles, which have spherical SiO_2 as the matrix phase, no $ZnFe_2O_4$ precipitates despite the presence of Zn and Fe, K and Cl, and no Ca, are presumed to have been formed by the above process.

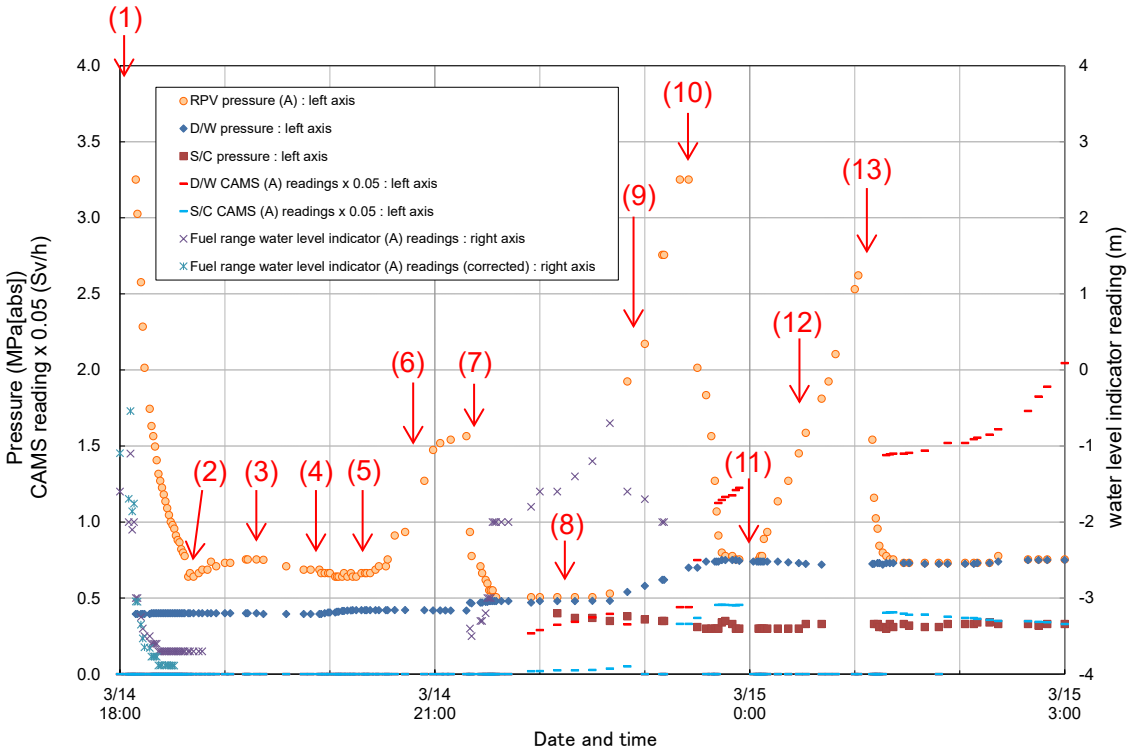

Figure 3　RPV pressure and other measured data after forced depressurization of Unit 2

■ 5. Discussion

As discussed above, assuming the In-RPV process as the formation process for Type A insoluble Cs particles not only explains the material origin of the Si, Zn, K, and Cl that make up the particles, but also identifies where and when they were formed; on the other hand, assuming the MCCI process does not explain why other natural mineral elements such as Ca and Al, which are part of the concrete constituent materials, and Na from seawater, cannot explain why other natural mineral elements are not present in appropriate proportions. However, the presence of Na in insoluble Cs particles was reported [22], and its influence was evaluated as follows. Table 4 shows the ratio of each element to Cl in insoluble Cs particles of type A [4],[5]. The K/Cl ratio in Type A is about 1 to 4, whereas the K/Cl ratio in seawater is more than two orders of magnitude lower. This suggests that seawater has little influence on the insoluble Cs particle composition in question.

Table 4 Ratio of each element to Cl in Type A insoluble Cs particles

Calculated from values in Yamaguchi et al. [4] and Kogure et al. [5]

Atomic ratio to Cl (-)

	Yamaguchi, et al. [4]		Kogure, et al. [5]					Sea water
	NWC-1	CB-8	P6-6 (ave.)	G3-8 (ave.)	W-01 (ave.)	P6-6 (center)	P6-6 (Cs-max)	
Si/Cl	29.2	61.8	85.8	34.8	36.2	158.3	55.5	
K/Cl	1.0	1.5	1.8	0.8	0.6	4.0	0.8	0.019
Fe/Cl	2.7	4.6	6.4	3.1	4.0	9.8	4.8	
Zn/Cl	3.4	7.1	6.9	4.8	5.2	9.7	5.6	
Rb/Cl	0.4	0.7	1.1	0.5	0.5	1.8	0.5	
Sn/Cl	0.2	0.5	0.9	0.7	0.7	1.0	0.9	
Cs/Cl	0.6	1.2	3.6	1.9	2.9	1.3	4.5	

Based on this assumption, the amount of insoluble Cs particles produced for Type A can be evaluated using the amount of K available for supply as follows. The results of the evaluation are shown in Table 5.

The total amount of inorganic zinc-containing paint applied to the interior walls of the Unit 2 S/C was approximately 2600 kg. The K content in this coating was about 0.12 wt%, which was 3.12 kg-K or 3.76 kg-K_2O. Based on the laboratory leaching test results, 0.752 kg-K_2O would be leached in 3000 m^3 of S/C water since about 20% of the K was leached. If 500 m^3 of water evaporated during RCIC operation in the RPV, 0.125 kg-K_2O would be deposited on the boiling surface. Since the percentage of K_2O present in Type A insoluble Cs particles is 1 wt%, it was evaluated that 12.5 kg of particles could form from this K_2O precipitate. Since the amount of Cs contained in Type A particles is at most 10 wt%, the

amount of Cs released as Type A is evaluated to be on the order of 1 kg. This is much less than the amount of Cs present in the core during the accident, which was about 200 kg. Here, the amount of SiO_2 required to form 12.5 kg of Type A insoluble Cs particles is about 70 wt% of the particle weight, as shown in Table 1, which is about 8.8 kg, or about 4 kg as Si content. On the other hand, assuming that Si forming insoluble Cs particles was supplied into the RPV from the inorganic Zn-containing coating film applied to the S/C inner surface, the amount of Si in the coating film (4-4.3 wt%) and Si leaching into the water (0.08-0.12), etc., is evaluated to be about 2 kg as the Si available for supply. This value is less than the amount of Si required to form 12.5 kg of insoluble Cs particles. It is suggested that the remaining Si is supplied from steel.

Table 5 Results of evaluation of the amount of K that can be supplied and the amount of insoluble Cs particles produced

Item	Evaluated value	
Coated area	8,566	m^2
Flat part fraction of coating film	0.8	m^2/m^2
Coating film thickness	100	μ m
Theoretical density of coating film	3.8	g/cm^3
Total amount of coating film	2,600	kg
Content of K in coating film	0.12	wt%
K in coating film	3.12	kg
K_2O in coating film	3.76	kg
Dissolved fraction of K into H_2O at 140 ℃	20	wt%-K
Dissolved K_2O into S/C water	0.752	kg
Water supplied into RPV	3,000	m^3
Evaporated water	500	m^3
K_2O into RPV	0.125	kg
K_2O content in a particle	1	%
Weight of Cs particles	12.5	kg

■ 6. Summary

The origin of elements and formation mechanism of Type A insoluble Cs particles, which were released into the environment due to the Fukushima Daiichi Nuclear Power Station accident and widely observed in the Fukushima and the metropolitan Tokyo areas, were discussed phenomenologically. Type A insoluble Cs particles have a glassy structure

that requires rapid cooling from high temperatures, and are thought to have formed in the RPV because they do not contain concrete constituents such as Ca. In addition, the presence of elements, such as Si, Zn, K, and Cl that were in the paint applied to the S/C inner surface, suggests that they were formed in the RPV of Unit 2, where the hot S/C water was introduced into the RPV.

The particles are estimated to have been formed under the condition that the fuel temperature was in the range of 1500°C to 2300°C and the FP content was Cs>>Ba. One of the most likely explanations is that the particles were formed around 21:00 on March 14, 2011, and released into the S/C at 21:20 on the same day when the SRVs were opened and quenched. Based on the amount of K in the paint that could have been the source, it was evaluated that about 10 kg order of particles or 1 kg-Cs_2O was produced. This is a very small amount compared to the total Cs content of about 200 kg.

Acknowledgments

The authors thank Dr. Yukihiko Sato, Dr. Katsumi Une, Dr. Masahiko Osaka, Prof. Yoshinao Kobayashi, Mr. Shiro Hikita, and Mr. Kenichiro Nozaki for valuable discussions on the chemistry of Cs-containing particles and the thermochemical behavior of fuel, fission products, and core materials at high temperatures during the Fukushima Daiichi Nuclear Power Station accident, and for the dynamic accident progress evaluation.

This research includes a part of the research funded by the Ministry of Economy, Trade and Industry of Japan under the "Subsidy for Decommissioning and Contaminated Water Countermeasures Project (Advancement of Comprehensive In-Reactor Situation Assessment)" in the FY2015 supplementary budget.

References

[1] K. Adachi, M. Kajino, Y. Zaizen and Y. Igarashi, Emission of spherical cesium-bearing particles from an early stage of the Fukushima nuclear accident, Scientific Reports, 2013; 3:2554: 1 - 5 ; DOI: 10.1038/srep02554.

[2] Y. Abe, Y. Iizawa, Y. Terada, et al., Detection of Uranium and Chemical State Analysis of Individual Radioactive Microparticles Emitted from the Fukushima Nuclear Accident Using Multiple Synchrotron Radiation X‐ray Analyses, Analytical Chemistry, 86(17) (2014) 8521 - 8525 ; dx.doi.org/10.1021/ac501998d.

[3] Y. Satou, K. Sueki, K. Sasa, et al., Analysis of two forms of radioactive particles emitted during the early stages of the Fukushima Dai-ichi Nuclear Power Station accident, Geochemistry Journal, 52 (2018) 137 - 143 ; DOI:10.2343/geochemj.2.0514.

[4] N. Yamaguchi, M. Mitome, et al., Internal structure of cesium bearing radioactive microparticles released from Fukushima nuclear power plant, Scientific Reports, 6:20548 (2016) 1 - 6 ; DOI: 10.1038/srep20548.

[5] T. Kogure, N. Yamaguchi, H. Segawa, et al., Constituent elements and their distribution in the radioactive Cs-bearing silicate glass microparticles released from Fukushima nuclear plant, Microscopy, 2016, 1 - 9 ; DOI: 10.1093/jmicro/dfw030.

[6] G. Furuki, J. Imoto, A. Ochiai, et al., Caesium-rich micro-particles: A window into the meltdown events at the Fukushima Daiichi Nuclear Power Plant, Scientific Reports, 7:42731 (2017) 1 - 10 ; DOI: 10.1038/srep42731.

[7] Y. Takahashi, H. Qin, C.M. Yeager and Q. Fan, Fukushima Review II on Migration of radionuclides from the Fukushima Daiichi Nuclear Power Plant accident, Geochemical Journal, 52 (2018) 81 - 83 ; DOI:10.2343/geochemj.2.0525.

[8] T. Okumura, N. Yamaguchi, T. Dohi, et al., Inner structure and inclusions in radio cesium-bearing microparticles emitted in the Fukushima Daiichi Nuclear Power Plant accident, Microscopy, 68(3) (2019) 234 - 242 ; DOI: 10.1093/jmicro/dfz004.

[9] K. Adachi, Shapes and Compositions of Insoluble Radioactive Particles from the Nuclear Accident, Earozoru Kenkyu, 32(4) (2017) 255 - 260 (in Japanese) ; DOI: 10.1093/jmicro/dfz004.

[10] S. Utsunomiya, G. Furuki, A. Ochiai, et al., Caesium fallout in Tokyo on 15th March, 2011 is dominated by highly radioactive, cesium-rich microparticles, arXiv: 1906.00212 (2019)

[11] A. Hidaka, Formation mechanisms of insoluble Cs particles observed in Kanto district four days after Fukushima Daiichi NPP accident, Journal of Nuclear Science and Technology, 56(9-10) (2019) 831 - 841 ; DOI: 10.1080/00223131.2019.1583611.

[12] Nuclear Regulation Authority, Progress of SGTS room inspection of units 1 to 4, 27 November 2020, (in Japanese). https://www.nsr.go.jp/data/000334477.

[13] T. Okumura, N. Yamaguchi, T. Dohi, et al., Loss of radioactivity in radio cesium-bearing microparticles emitted from the Fukushima Dai-ichi nuclear power plant by heating, Scientific Reports, 10:1038 (2018) 1 - 8 ; DOI:10.1038/s41598-018-28087-5.

[14] IRID and IAE, Upgrading for Identifying Conditions Inside the Reactor, June, 2018 (from IRID home page, in Japanese): https://irid.or.jp/_pdf/20170000_01.pdf

[15] Y. Ohishi, F. Nakamori, H. Muta et al., Investigation of in-reactor cesium chemical behavior in TEPCO's Fukushima Daiichi Nuclear Power Station accident (6) Simulation

study on microstructure of Cs-bearing particle, 2018 Annual meeting of AESJ., Osaka (2018), 2M16 (in Japanese).

[16] F. Nakamori, Y. Ohishi, H. Muta et al., Investigation of in-reactor cesium chemical behavior in TEPCO's Fukushima Daiichi Nuclear Power Station accident (7) Leaching behavior of Zn, Si and other elements from inorganic Zn-rich paint, 2018 Annual meeting of AESJ., Osaka (2018), 2M17 (in Japanese).

[17] H. Kleykamp, The chemical state of the fission products in oxide fuels, J. Nucl. Mater, 131(2-3) (1985) 221 - 246 ; doi.org/10.1016/0022-3115(85)90460-X.

[18] Y. Pontillon and G. Ducros, Behavior of fission products under severe PWR accident conditions: the VERCORS experimental program - Part 2: release and transport of fission gases and volatile fission products, Nucl. Eng. Des., 240 (2010) 1853 - 1866 ; doi.org/10.1016/j.nucengdes.2009.06.024. C.R. Martial, J. Sercombe and Y. Pontillon, TopFuel 2018 A0139.

[19] K. Une and S. Kashibe, Fission Gas Release during Post Irradiation Annealing of BWR Fuels, J. Nucl. Sci. Technol., 27(11) (1990) 1002 - 1016 ; DOI: 10.1080/18811248.1990.9731285.

[20] JAEA, FY2016 Report on the Results of the Project commissioned by Nuclear Regulation Authority, Advanced source term evaluation technology during sever accidents, 2017 (from NRA home page, in Japanese): https://www.nsr.go.jp/data/000210758.pdf

[21] M. Steinbrück, B_4C Control Rod Behavior during Severe Accident Sequences, International Conference, Nuclear Energy for Central Europe 2003, Portorož, Slovenia, September 8 - 11, 2003.

[22] T. Okumura, N. Yamaguchi, H. Suga, et al., Reactor environment during the Fukushima nuclear accident inferred from radiocaesium-bearing microparticles, Scientific Reports (2020) 10:1352: https://doi.org/10.1038/s41598-020-58464-y.